Studies on Crystalline Structures of Two-dimensional Covalent Organic Frameworks

GAO, Jia

Doctor of Philosophy

Department of Structural Molecular Science
School of Physical Sciences
SOKENDAI (The Graduate University for Advanced Studies)

Studies on Crystalline Structures of Two-dimensional Covalent Organic Frameworks

二次元共有結合性有機骨格の結晶構造に関する研究

GAO, Jia

Department of Structural Molecular Science

School of Physical sciences

SOKENDAI

Contents

Chapter 1

General Introduction

1.1 Background

Porous materials have attracted great attention due to their unique structures, exceptional properties and versatile applications. During the last decades, porous materials have been evolved not only in structures but also in properties and functions. Their composition, structure, chemical and physical properties are synthetically tunable. Nanoporous frameworks with extended structures such as zeolites[1)], metal-organic frameworks (MOFs)[2-5)] and conjugated microporous polymers (CMP)[6, 7)] open great potential for various applications with great advantages over traditional or conventional processes. Catalysis[8-10)], gas adsorption[11-12)], sensors[13)] and photovoltaics[14)] are the most prominent targets.

Organic compounds are cost-efficient, producible at large scale and can be easily modified using various organic reactions. Hence, developing functional porous materials based on organic structures is highly desirable. Organic porous materials such as CMPs and porous organic frameworks (POFs)[15)] exhibit large surface areas, high pore volumes and excellent physicochemical stability. However, those materials are usually obtained as amorphous organic networks that have limited or even no long-range orderings. This amorphous issue raises challenges in the correlation of structure–property relationships and leads to the difficulty in providing suitable models for rational structural and function designs. In this sense, a class of organic porous materials with

high crystallinity and long-range molecular orderings is high desirable.

In 2005, Yaghi and co-workers first developed a crystalline porous organic polymer named covalent organic frameworks (COFs) for gas adsorption[16]. During this ten years, many groups worldwide have involved the design, synthesis and functional explorations, greatly expanding the structural scopes and functional diversities of COFs[17-25]. COFs are a class of organic, crystalline and porous polymers that are liked by using covalent bonds and are composed of lightweight elements, including hydrogen, boron, carbon, nitrogen and oxygen, thus serving as a new series of porous materials for gas adsorption[26-30].

In the case of first COF examples including COF-1 and COF-5, the condensation of planar boronic acids and phenol derivatives leads to the formation of these two dimensional (2D) COFs. The 2D layers are held together by London dispersion interactions and form a lamellar structure via stacking. Unlike Bernal stacking mode observed for graphite, COF-1 and COF-5 were reported to adopt AB (space group $P6_3/mmc$) and AA (space group *P6/mmm*) stacking, respectively **(Figure 1. 1)**. These crystalline structures have been resolved using powder X-ray diffraction (PXRD) together with structural simulations.

In 2007, the group of Yaghi reported the synthesis of three-dimensional (3D) COFs **(Figure 1. 2)**[31]. 3D COFs are of particular interest for their very low mass density and high porosity. Similar to 2D

COFs, condensation of boronic acids and hydroxyphenyl compounds led to the formation of COF-102, 103, 105, 108 and 202.[31, 32] All of these 3D COFs adopt ***ctn*** topology, whereas COF-108 that has the same composition as that of COF-105 assumes ***bor*** topology. COF-300 formed from tetragonal and linear building units, possesses diamond topology and has been reported to have five-fold interpenetrated network structure.[33] Unlike 3D MOFs, the connectors in 3D COFs are not metal oxide clusters, but covalently bound organic moieties. In 3D COFs, the centers of the tetragonal blocks were either *sp*3 carbon or silicon atoms.

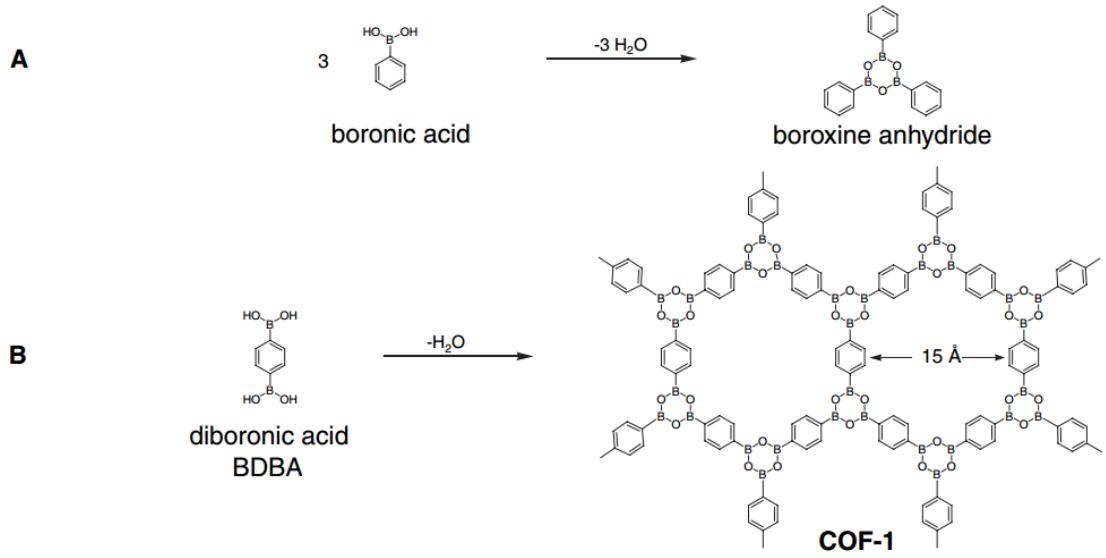

Figure 1. 1. The synthesis route and framework of COF-1[16].

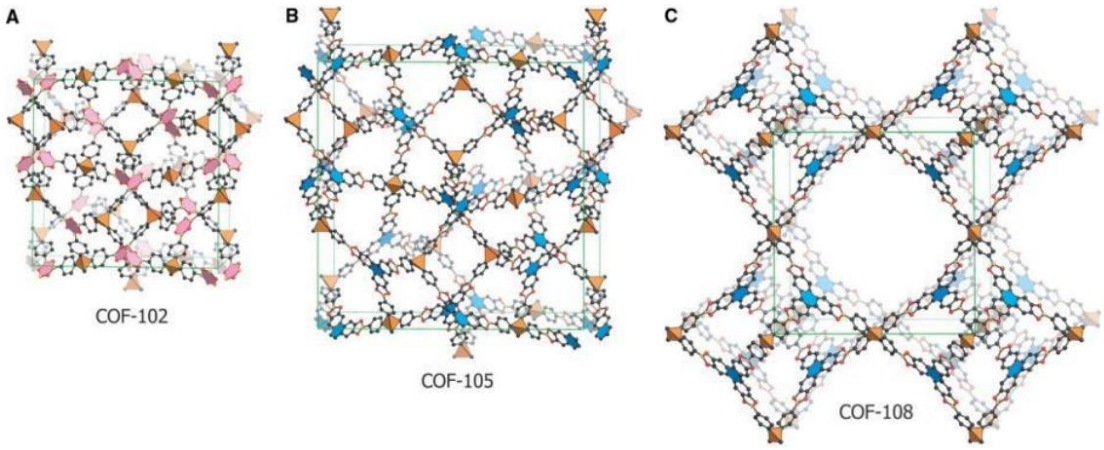

Figure 1. 2. Modeled crystalline structure of A) COF-102, B) COF-105 and C) COF-108[31)].

The key to assemble a crystalline organic framework is considered to gain thermodynamic control over the reaction. With this notion, it is possible to overcome the crystallization problem in the long expansion distance for the covalently linked structures. This is accomplished by striking a balance between the kinetic and thermodynamic factors to induce reversible covalent bond formation, a necessary criterion to crystallize extended structures.

The design principle of COFs is known as reticular chemistry[34)]. Desired materials can be realized by starting with well-defined and rigid molecular building blocks that will maintain their structural integrity throughout the construction process. The extended structures adopt highly symmetric topologies. The synthetic route follows well-defined conditions and enables a control over the instinct characters of the

resulting materials. In short, it is the chemistry of linking molecular building blocks by strong bonds into predetermined structures. The knowledge about how atoms organize themselves during synthesis is essential for the design. The principal possibilities rely on the starting compounds and the reaction mechanisms. Porosity is almost an inevitable outcome of reticular synthesis. Solvents may be used in most cases as space filling agents and in cases of more than one possibility as structure-directing agents.

Thousands of materials have been synthesized using the reticular chemistry principles[35, 36]. The scheme defines nets as the collection of vertices and edges that form an irreducible network in which any two vertices are connected through at least one continuous path of edges (**Figure 1. 3**). Building units are finite nets as in the case of a polyhedron. Periodic structures have one, two or three-periodic nets[37-41].

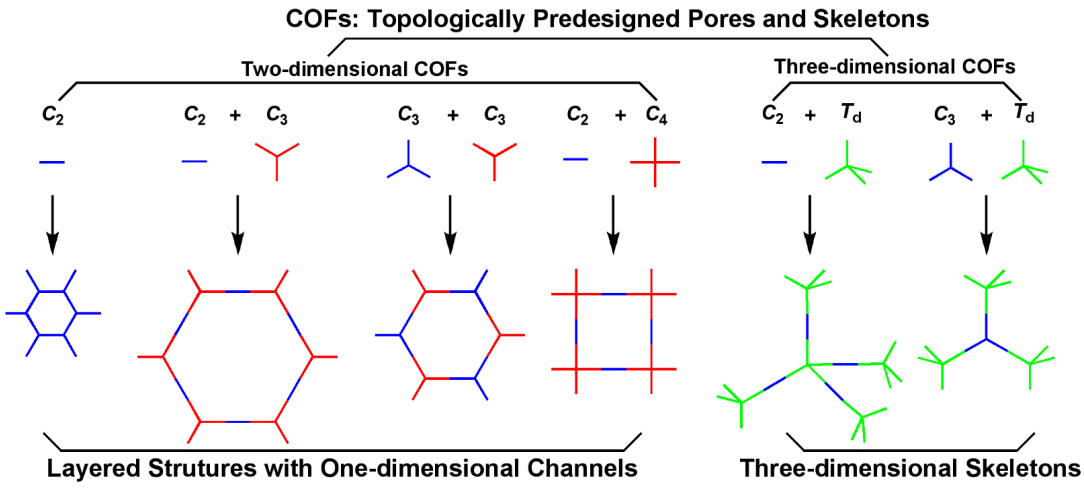

Figure 1. 3. Predesign principle of COF using reticular chemistry[41].

1.2 Structural Characterizations

Appropriate characterizations are the key to the deep understanding of the structural essence of COF materials. Many characterization techniques have been applied to the research work of 2D COFs, including PXRD, scanning electron microscopy (SEM), transmission electron microscopy (TEM), infrared spectroscopy (IR), nuclear magnetic resonance spectroscopy (NMR), electronic absorption spectroscopy, fluorescence, gas sorption, thermogravimetric analysis (TGA) and so on. Among these characterization methods, the ones that directly inform the crystalline properties of 2D COFs are PXRD, TEM and polarizing light microscopy (PLM). The main experiments of this thesis are conducted using the above three techniques.

1.2.1 X-Ray Diffraction

X-Ray is a kind of electromagnetic radiation with typical wavelengths from 5 pm up to 100 pm, which lies between UV-light and gamma radiation. Generally, X-rays are generated when a cold metal target is bombarded with accelerated, focused high-energy electrons[42-44)]. Collision of the electrons with a specimen leads to an emission of a continuous spectrum of X-rays. In addition to white radiation, characteristic radiation is produced as well, resulting from X-ray fluorescence. An emitting electron creates a hole in the inner shell of the

atom, which is filled subsequently by an electron from an outer shell. The energy difference of these two energy states of the transferred electron is emitted as X-ray photon. The wavelength and intensity of the fluorescent X-rays depend on the target material, since energy differences between the electron shells are variable.

To achieve a monochromatic parallel beam, different metal filters and a collimator are applied to selectively isolate an intense part of the spectrum, usually *Kα* radiation. Incidence of a monochromatic beam of X-ray photons onto a specimen results in three basic phenomena, which are absorption, scattering and reflection. The X-ray diffraction technique is based on analysis of reflected X-ray from specimen to acquire the structural information of specimens.

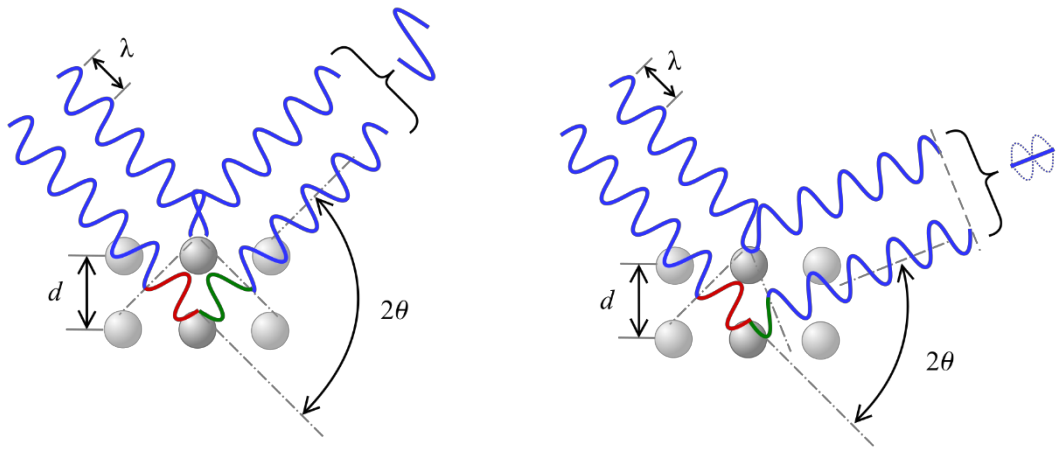

Figure 1. 4. The basic principle of x-ray diffraction of Bragg's law.

X-ray diffraction is based on constructive interference of monochromatic X-rays and a crystalline sample (**Figure 1. 4**). These X-rays are generated by a cathode ray tube or target, filtered to produce monochromatic radiation, collimated to concentrate, and directed penetrate the sample. The interaction of the incident rays with the sample produces constructive interference (and a diffracted ray) when conditions satisfy the Bragg's Law ($n\lambda = 2d\sin\theta$). This law relates the wavelength of electromagnetic radiation to the diffraction angle and the lattice spacing in a crystalline sample. These diffracted X-rays are then detected, processed and counted. By scanning the sample through a range of 2θ angles, all possible diffraction directions of the lattice should be attained due to the random orientation of the powdered material **(Figure 1. 5)**.

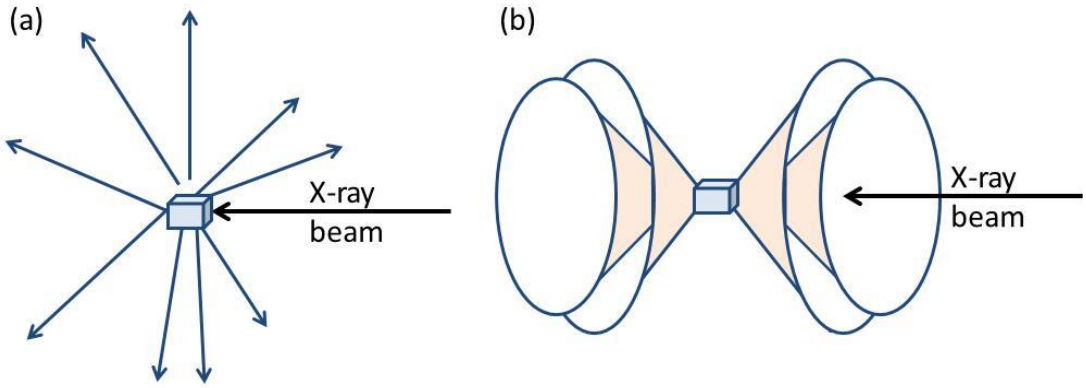

Figure 1. 5. Diffraction pattern from a) single crystal particle and b) polycrystalline sample.

1.2.2 Transmission Electron Microscope

The transmission electron microscope (TEM) uses a high voltage electron beam to create an image[45, 46]. The electron beam is produced with electron gun, commonly adapted a tungsten filament cathode as the electron source. The electron beam is accelerated by an electrostatic field typically over 100 k eV, focused by electrostatic and electromagnetic lenses, and transmitted through the specimen that is in part transparent to electrons. When electron beam penetrates the specimen, it carries information about the structure of the specimen that is magnified by the objective lens system of the microscope. The spatial variation in this information may be viewed by projecting the magnified electron image onto a fluorescent viewing screen coated with a phosphor or scintillator material such as zinc sulfide. Alternatively, the image can be photographically recorded by exposing a photographic film or plate directly to the electron beam. As the technology advances, the image from TEM can be collected in teal-time by means of a lens optical system combining with a fiber optic light-guide to the sensor of a CCD (charge-coupled device) camera. The image detected by the CCD can be displayed on a monitor or computer.

Resolution of the TEM is limited mainly by spherical aberration. Recently, a new generation of aberration correctors have been applied to partially overcome spherical aberration. Systematic optical correction of spherical aberration for the high-resolution transmission electron

microscopy (HR-TEM) has allowed the resolution of images reach below 0.5 angstrom and magnifications above 50 million times. The ability to determine the positions of atoms within materials has made the HR-TEM a powerful tool for nano-technologies research.

Transmission electron microscopes are also used in electron diffraction mode. The advantages of electron diffraction over X-ray crystallography are that the specimen need not be a single crystal or even a polycrystalline powder. The Fourier transformation reconstruct the object's magnified structure physically and thus avoids the need for solving the phase problem faced by the X-ray crystallographers after achieving the X-ray diffraction patterns of a single crystal or polycrystalline powder. The major disadvantage of the transmission electron microscope is the need for extremely thin sections of the specimens, typically about 100 nanometers. Sections of biological specimens, organic polymers and similar materials may require special treatment with complicated preparation techniques in order to achieve the required image contrast.

1.2.3 Polarizing Light Microscopy

The vibration direction of light is perpendicular to the progressing light. Light from an ordinary light source (natural light) that vibrates in random directions is called nonpolarized light[47]. In contrast, while light with vertical vibration that travels within a single plane is called linearly polarized light. The use of polarized light on the optical microscope allows us to determine the optical crystallographic properties of the crystal and those optical microscopes with appreciate devices, which can conduct in observation polarized light mode, is Polarized Light Microscopy (PLM). Up to now, most research microscopes provide polarizing mode as a basic function.

A polarizing plate (polarizing filter) or polarizing prism is often used as the device (polarizer) to change natural light to linearly polarized light. Configuring the primary and secondary polarizing devices in the orthogonal directions of each transmitting linearly polarized ray will cut the light completely. Such state in which the primary light polarizing device is the polarizer and the secondary device is the analyzer.

Some of crystals can occur double refraction or birefringence phenomenon when light pass through them. It means that the incident is divided into two linearly polarized light that have mutually crossing vibration directions. Between these two light rays, the one that follows the law of refraction is called an ordinary ray, while the other one is

called an extraordinary ray. Their speed and index of refraction differ from one another. A crystal that can occur birefringence phenomenon is called anisotropic crystal. However, toward a certain direction, double refraction phenomenon does not occur. This direction is named as optical axis. Polarized light microscopy provide research a powerful means to measure birefringence.

1.3 Aim of This Thesis

After ten years' development, the studies on 2D COF have gained a great success on structural design, synthesis and functional exploration. However, the understanding about the crystalline structure of 2D COF need further improvement. The solution of this important issue would bring new opportunity to the COF field and would contribute to the further development of the field.

Based on the above background, in this thesis, the author utilized multiple methods combing the experimental and theoretical aspects with an aim to give different explanations on some experimental phenomenon that cannot be perfectly illustrated with existing 2D COFs structural models. This thesis is to develop a comprehensive, rational structural theoretical model to give a rational interpretation on the crystalline essence of 2D COFs.

1.4 References

1) M. E. Davis, *Nature*, 2002, **417**, 813.

2) J. R. Long and O. M. Yaghi, *Chem. Soc. Rev.*, 2009, **38**, 1213.

3) M. O'Keeffe, *Chem. Soc. Rev.*, 2009, **38**, 1215.

4) D. J. Tranchemontagne, J. L. Mendoza-Corte´ s, M. O'Keeffe and O. M. Yaghi, *Chem. Soc. Rev.*, 2009, **38**, 1257.

5) J. J. Perry IV, J. A. Perman and M. J. Zaworotko, *Chem. Soc. Rev.*, 2009, **38**, 1400.

6) A. I. Cooper, *Adv. Mater.*, 2009, **21**, 1291.

7) J.-X. Jiang, F. Su, A. Trewin, C. D. Wood, N. L. Campbell, H. Niu, C. Dickinson, A. Y. Ganin, M. J. Rosseinsky, Y. Z. Khimyak and A. I. Cooper, *Angew. Chem., Int. Ed.*, 2007, **46**, 8574.

8) G. Wu, K. L. More, C. M. Johnston and P. Zelenay, *Science*, 2011, **332**, 443.

9) Farha, O. K.; Spokoyny, A. M.; Hauser, B. G.; Bae, Y.-S.; Brown, S. E.; Snurr, R. Q.; Mirkin, C. A.; Hupp, J. T. *Chem. Mater.*, 2009, **21**, 3033.

10) A. Corma, *Chem. Rev.*, 1997, **97,** 2373.

11) J. Graetz, *Chem. Soc. Rev.*, 2009, **38**, 73.

12) M. P. Suh, H. J. Park, T. K. Prasad and D.-W. Lim, *Chem. Rev.*, 2012, **112**, 782.

13) D. Jiang., T. Aida*., Prog. Polym. Sci*., 2005, **30**, 403.

14) S. Wan, J. Guo, J. Kim, H. Ihee and D. Jiang, *Angew. Chem., Int. Ed.*, 2008, **47**, 8826.

15) P. Pandey, A. P. Katsoulidis, I. Eryazici, Y. Y. Wu, M. G. Kanatzidis and S. T. Nguyen, *Chem. Mater.*, 2010, **22**, 4974.

16) A. P. Cote, A. I. Benin, N. W. Ockwig, M. O'Keeffe, A. J. Matzger and O. M. Yaghi, *Science*, 2005, **310**, 1166.

17) R. W. Tilford, W. R. Gemmill, H.-C. zur Loye and J. J. Lavigne, *Chem. Mater.*, 2006, **18**, 5296.

18) M. Dogru, A. Sonnauer, A. Gavryushin, P. Knochel and T. Bein, *Chem. Commun.*, 2011, **47**, 1707.

19) E. L. Spitler, B. T. Koo, J. L. Novotney, J. W. Colson, F. J. Uribe-Romo, G. D. Gutierrez, P. Clancy and W. R. Dichtel, *J. Am. Chem. Soc.*, 2011, **133**, 19416.

20) E. L. Spitler and W. R. Dichtel, *Nat. Chem.*, 2010, **2**, 672.

21) E. L. Spitler, J. W. Colson, F. J. Uribe-Romo, A. R. Woll, M. R. Giovino, A. Saldivar and W. R. Dichtel, *Angew. Chem., Int. Ed.*, 2012, **51**, 2623.

22) S. Wan, F. Gandara, A. Asano, H. Furukawa, A. Saeki, S. K. Dey, L. Liao, M. W. Ambrogio, Y. Y. Botros, X. Duan, S. Seki, J. F. Stoddart and O. M. Yaghi, *Chem. Mater.*, 2011, **23**, 4094.

23) S. Kandambeth, A. Mallick, B. Lukose, M. V. Mane, T. Heine and R. Banerjee, *J. Am. Chem. Soc.*, 2012, **134**, 19524.

24) B. P. Biswal, S. Chandra, S. Kandambeth, B. Lukose, T. Heine and R. Banerjee, *J. Am. Chem. Soc*., 2013, **135**, 5328.

25) S.-Y. Ding, J. Gao, Q. Wang, Y. Zhang, W.-G. Song, C.-Y. Su and W. Wang, *J. Am. Chem. Soc.*, 2011, **133**, 19816.

26) F. J. Uribe-Romo, C. J. Doonan, H. Furukawa, K. Oisaki and O. M. Yaghi, *J. Am. Chem. Soc.*, 2011, **133**, 11478.

27) X. Feng, L. Liu, Y. Honsho, A. Saeki, S. Seki, S. Irle, Y. Dong, A. Nagai and D. Jiang, *Angew. Chem., Int. Ed.*, 2012, **51**, 2618.

28) X. Feng, L. Chen, Y. Honsho, O. Saengsawang, L. Liu, L. Wang, A. Saeki, S. Irle, S. Seki, Y. Dong and D. Jiang, *Adv. Mater.*, 2012, **24**, 3026.

29) S. Jin, X. Ding, X. Feng, M. Supur, K. Furukawa, S. Takahashi, M. Addicoat, M. E. El-Khouly, T. Nakamura, S. Irle, S. Fukuzumi, A. Nagai and D. Jiang, *Angew. Chem., Int. Ed.*, 2013, **52**, 2017.

30) M. Dogru, M. Handloser, F. Auras, T. Kunz, D. Medina, A. Hartschuh, P. Knochel and T. Bein, *Angew. Chem. Int. Ed.*, 2013, **125**, 2992.

31) H. M. El-Kaderi, J. R. Hunt, J. L. Mendoza-Cortes, A. P. Co ˆte ´, R. E. Taylor, M. O'Keeffe and O. M. Yaghi, *Science*, 2007, **316**, 268.

32) J. R. Hunt, C. J. Doonan, J. D. LeVangie, A. P. Cote and O. M. Yaghi, *J. Am. Chem. Soc.*, 2008, **130**, 11872.

33) F. J. Uribe-Romo, J. R. Hunt, H. Furukawa, C. Klock, M. O'Keeffe and O. M. Yaghi, *J. Am. Chem. Soc.*, 2009, **131**, 4570.

34) O. M. Yaghi, M. O'Keeffe, N. W. Ockwig, H. K. Chae, M. Eddaoudi and J. Kim, *Nature*, 2003, **423**, 705.

35) M. O'Keeffe, M. A. Peskov, S. J. Ramsden and O. M. Yaghi, *Acc. Chem. Res.*, 2008, **41**, 1782.

36) http://rcsr.anu.edu.au/

37) O. Delgado-Friedrichs and M. O'Keeffe, *J. Solid State Chem*., 2005, **178**, 2480.

38) O. Delgado-Friedrichs, M. D. Foster, M. O'Keeffe, D. M. Proserpio, M. M. J. Treacy and O. M. Yaghi, *J. Solid State Chem.*, 2005, **178**, 2533.

39) M. O'Keeffe and O. M. Yaghi, *Chem. Rev.,* 2012, **112**, 675.

40) D. J. L. Tranchemontagne, Z. Ni, M. O'Keeffe and O. M. Yaghi, *Angew. Chem., Int. Ed.*, 2008, **47**, 5136.

41) X. Feng, X. Ding and D. Jiang, *Chem. Soc. Rev*., 2012, **41**, 6010.

42) A. R. Barron, *Physical Methods in Chemistry and Nano Science.* Rice University: 2012.

43) D. E. McGee, *Practical Protein Crystallography.* San Diego, Academic Press: 1993.

44) W. Massa, *Crystal Structure Determination.* Berlin: Springer: 2004.

45) R. Egerton, *Physical principles of electron microscopy.* Springer: 2005.

46) L. Reimer and H. Kohl, *Transmission Electron Microscopy: Physics of Image Formation.* Springer: 2008.

47) M. Abramowitz, *Microscope Basics and Beyond.* Olympus America Inc.: 2003.

Chapter 2

Spatially Confined Guest Molecules and Their Impacts on Crystalline Structures of Covalent Organic Frameworks

"Covalent organic frameworks with spatially confined guest molecules in nanochannels and their impacts on crystalline structures"

Jia Gao and Donglin Jiang*

Chemical Communications, 2016, **52**, 1498.

Abstract

In this chapter, the author demonstrated profound effects of spatially confined guest molecules in one-dimensional nanochannels on X-ray diffraction behaviors of covalent organic frameworks. The results give insights into the abnormal X-ray diffraction patterns and suggest a novel molecular dynamic strategy for resolving crystalline structures of covalent organic frameworks.

2. 1 Introduction

Covalent organic frameworks (COFs) is an emerging class of porous crystalline polymers in which organic building blocks are covalently linked to form extended structures with periodicities[1-5]. In two-dimensional (2D) COFs, vertices and edges are topologically linked in a 2D manner to yield monolayers. The 2D monolayers crystallize and stack via interlayer π-π interactions to form lattice structures. Accordingly, the lattice symmetry of 2D-COFs can be divided into two levels in relation to their two structural hierarchies [6-16]. One level is the intrinsic symmetry of 2D polymer monolayer, which is controlled by the structures of organic building blocks and the topological diagram. Another level is the spatial symmetry that is determined by the π-stacking orders of 2D polymer layers. The differences of both two levels give rise to different global structural symmetry and yield different powder X-ray diffraction (PXRD) patterns. Although the PXRD pattern could provide essential data set for structural analysis and simulations, however, the absence of single crystals enhances the difficulty in identifying a suitable stacking structure for each member of COFs. Heine et. al. has reported the different stacking modes of a variety of COFs and provided insights into the structural effects on stacking energy and PXRD patterns[17].

In 2D-COFs, two distinct stacking orders are usually considered. One is eclipsed arrangement (AA stacking) in which atoms of adjacent

layers lie directly over each other. Another one is a staggered arrangement (AB stacking) that can be regarded as two adjacent layers offset against each other by a distance of half of the unit cell. In literature, except one example, all of 2D COFs adopt AA stacking. Lukose *et al.* calculated the total energy of COFs in different stacking arrangement and found that AB stacking is energetically less favorable than the AA stacking[17-20]. COF-1 **(Figure 2. 1)** is the smallest family of COFs and it was found to exhibit unique PXRD patterns under different conditions such as in the presence or absence of guest molecules. The stacking structure of COF-1 has been reported to be staggered AB mode[3].

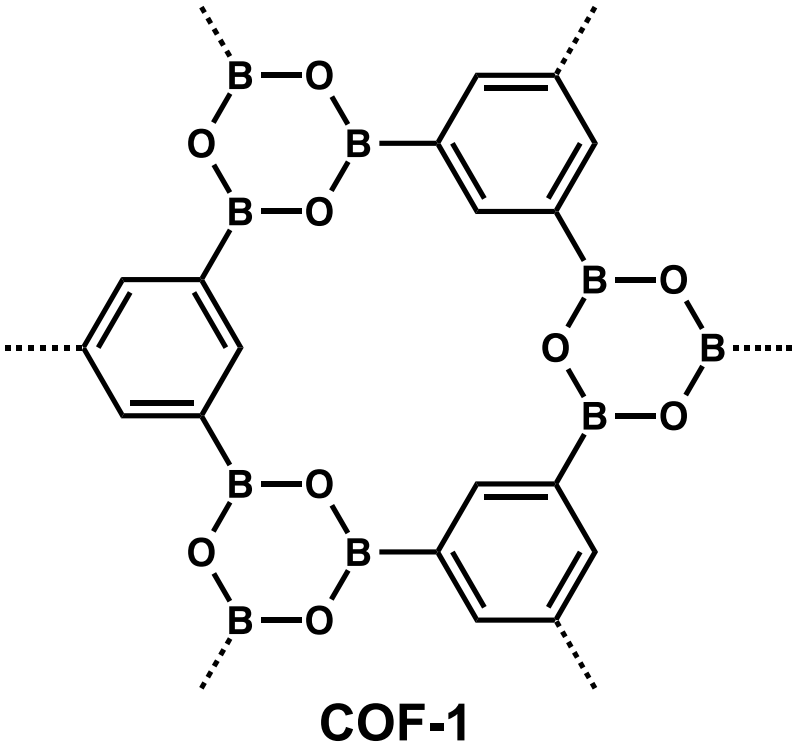

Figure 2. 1. Chemical structure of COF-1.

One-dimensional open channels are the structural bases for COFs to

accommodate guest molecules. In this study, the author focused on the host–guest interactions and managed to elucidate the relationship between the guest confinement in the channels and the variation of PXRD patterns. To clarify the systems, the author utilized a COF with the smallest pore, COF-1[1b)] and filled the channels with different contents of guest molecules, to show the effects of guest molecules on the PXRD patterns via molecular dynamic simulations. In this chapter, the author employs simulation methods together with the theoretical analysis to reveal the correlation between the structure features and PXRD spectra of COF-1.

2. 2 Experimental

PXRD simulation was performed using the Reflex Module as implemented in Materials Studio 4.4[21)]. Scanning ranges between 5° and 25° with a step size of 0.02°. Cu Ka_2 radiation was not considered for clarity. For each structure, the author adopted previously reported structural parameters in literature for modeling their different configurations[3, 7)]. As for the guest packing structures, an additional line broadening factor was brought in with mean crystallite size at 1×10^3 nm for imitating the experimental PXRD spectra.

Molecular Mechanics (MM) and Molecular Dynamics (MD) calculations were performed using Forcite programs implemented in Materials Studio 4.4 and combined force field (vdW-FF plus Dreiding)[22)].

The Validation of the Dreiding force field has been proofed. A cutoff of 1.8 nm was used to calculate the LJ interactions and short-range electrostatic interactions. The long-range electrostatic interactions were evaluated using the Particle-Mesh Ewald (PME) algorithm[23] with an accuracy tolerance of 10^{-5} kcal mol^{-1}. The supercell for calculations was 3 × 3 × 10 and periodic boundary conditions were exerted in three dimensions. Molecular dynamics calculations were performed for simulating the thermal fluctuations in actual environment, which cause each layer stacking in a random direction **(Figure 2. 2)**. For each MD simulation, we started with the equilibrium geometry after 5000 steps of conjugated gradient (CG) minimization (cell parameters and atom positions) followed by 100 ps of NVT dynamics to heat the system to 398 K. Finally, the author ran NPT dynamics at 1 atm and 398 K for 2.0 ns. After the MD simulation, the free volume was marked out with Connolly surface that is the territory of guest molecules padding. Mesitylene molecules were packed into the individual pores respectively to represent the random population in as-synthesized COF-1 sample. Based on the sum of guest molecules in each pores, the author evaluated the overall amount of mesitylene filled in supercell with the average-padding density of mesitylene that surrounded in Connolly surface[24]. It is obviously that those results beyond the experimental density of mesitylene liquid (0.864 g cm^{-3} at 298 K) have no physical meaning. Nevertheless, based on our

simulation, there still exists 14% of the free space unoccupied with mesitylene when padding density reach 0.8 g cm^{-3}. Hence, the author set the upper limit of packing density to 0.9 g cm^{-3} **(Figure 2. 3)**.

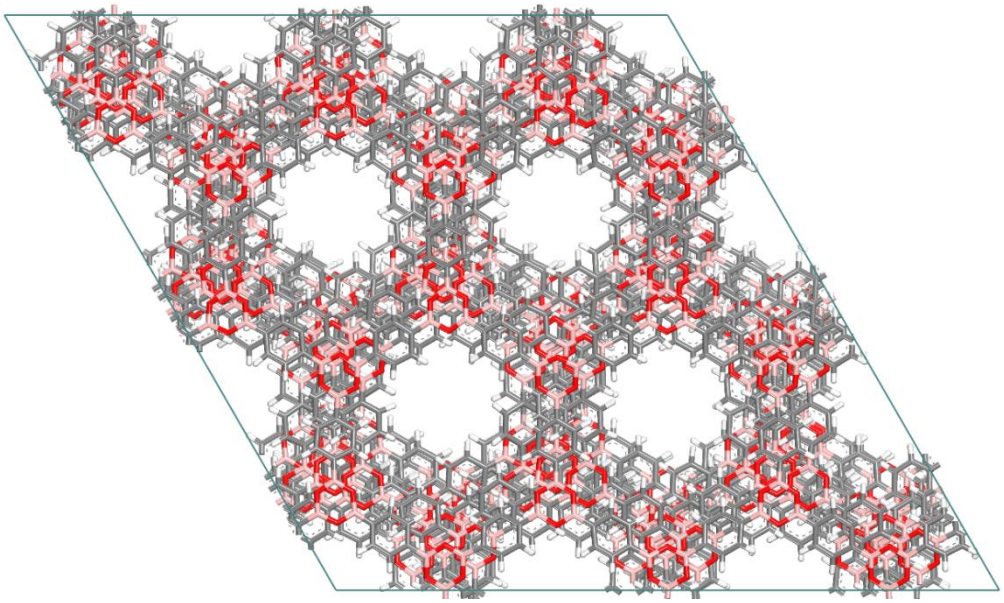

Figure 2. 2. A snapshot of COF-1 supercell in MD simulation.

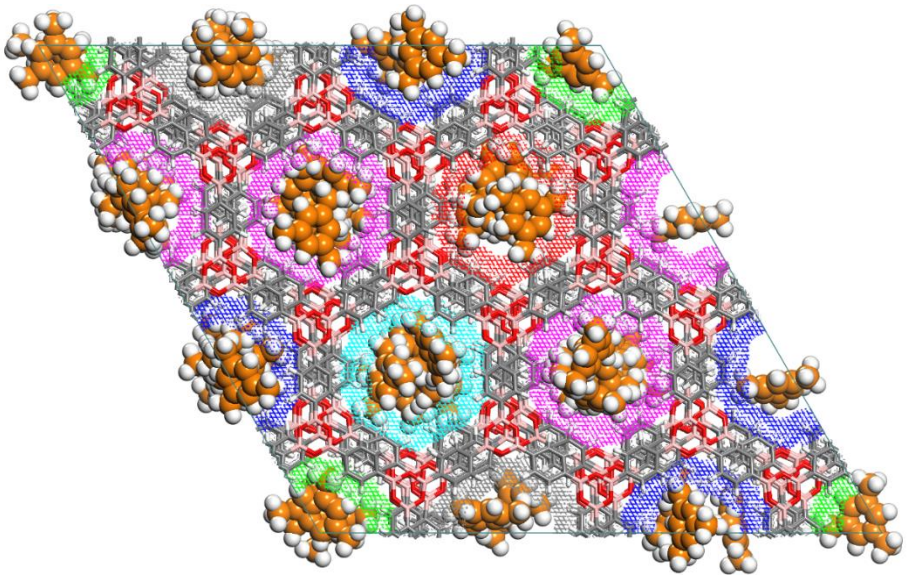

Figure 2. 3. A snapshot that mesitylene in the pores of AA COF-1. The average packing density is about 0.5 g cm^{-3}.

2. 3 Results and Discussion

The hexagonal texture of COF-1 gives rise to typical PXRD peaks that are assignable to 100, 110, and 200 facets. One of the noteworthy features that make COF-1 a distinct case is an odd (110) peak with abnormal high intensity comparing with the other two. Whereas given that (200) peak comes from the second-order diffraction of (100) facet, the author only adopts (100) and (110) as indexing peaks to study the mechanism of how the unique PXRD patterns of COF-1 form in experiment. The ratio of the intensity between (110) peak and (100) peak, $I_{(110)}/I_{(100)}$ is defined as an index to monitor the change of PXRD spectra.

In order to investigate the relationship between the stacking configurations of the interlayers and the intensities variation of (100) and (110), COF-1 together with COF-5, another typical 2D COF with primitive hexagonal lattice, was rebuilt in AA stacking order without any external molecule in pores. The author shifted every second layer along zigzag vertices of the hexagonal pores to see the changes of the PXRD spectra because zigzag mode only changes the overall intensity distribution of XPRD patterns but without introducing any shifting or splitting into individual peaks. The initial and the final stacking is AA stacking (*P*6/*mmm*) while AB stacking ($P6_3/mmc$) can occur twice during the overall offsetting process.

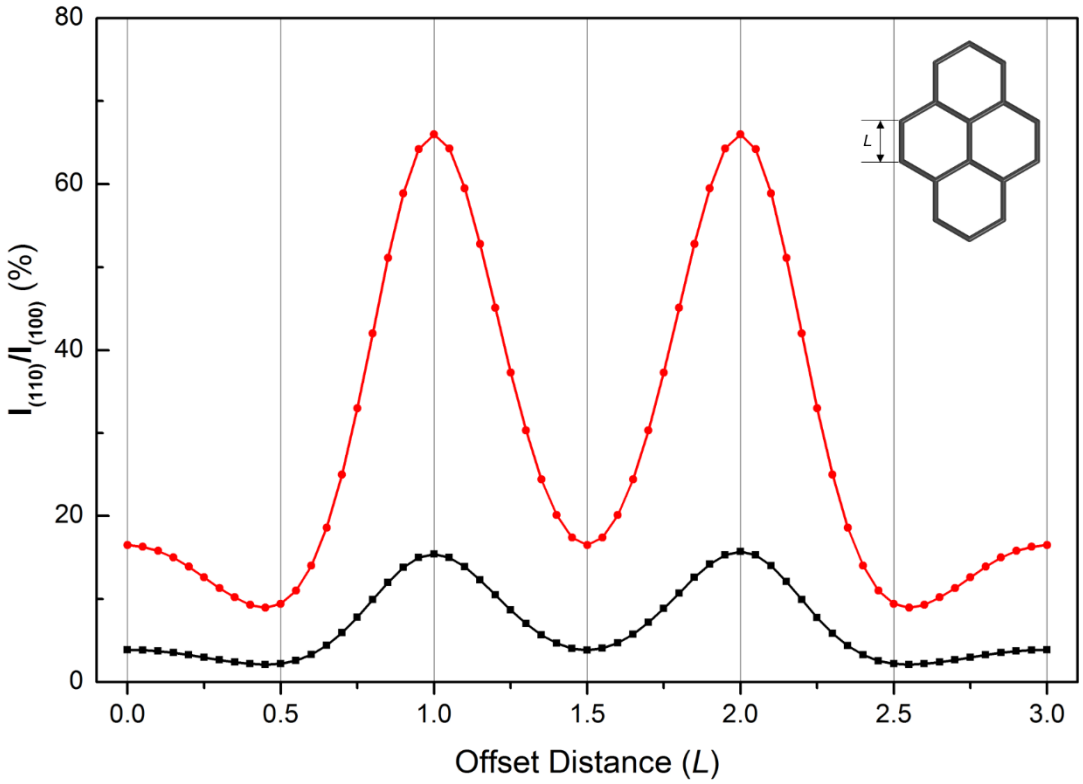

Figure 2. 4. Variation curve of $I_{(110)}/I_{(100)}$ (COF-1: black curve; COF-5: red curve) by shifting adjacent layers in zigzag direction. Offset distance (*L*) is defined as the edge length of a hexagonal pore.

Figure 2. 4. shows the variation curve of intensity ratio of $I_{(110)}/I_{(100)}$ corresponding to the shifting distance changes. The intensity of (110) reflection is reduced gradually when the arrangement drifts from AA stacking and then reaches the minimum when approaching the midpoint from AA stacking to AB stacking. With the configuration drawing near the AB stacking, the signal strength of (110) rises sharply and then climbs up to the summit when perfect staggered stacking is formed. To our surprise, the intensity of (110) reflection reaches the maximum with only

15.4 % of the (100) intensity in AB stacking even weaker than COF-5 in AA stacking, which cannot match with the currently available experimental data. Apparently, the PXRD pattern of COF-1 in AB stacking show no obvious distinction with other COFs **(Table 2. 1)** and there must exist some other factors causing the abnormal enhancement of (110) reflection.

The pores of as-synthesized COF-1 were reported to be occupied by mesitylene. Given this detailed experimental evidence, the author built up four types of COF-1 structural models and then generated their simulated PXRD spectra for comparison. (i) AA stacking without mesitylene molecule in the pore; (ii) AB stacking without mesitylene molecules in the pores; (iii) AA stacking with mesitylene molecules in the pores; (iv) AB stacking with mesitylene molecules in the pores **(Figure 2. 5)**. The result is interesting: no matter what arrangements are taken, the structures within the mesitylene always show more similarity than those without mesitylene in. Our simulation demonstrated that mesitylene molecules filling into the as-synthesized COF-1 is a more critical factor in forming a unique PXRD pattern than the AB stacking order.

Table 2. 1. The structural parameters and the relative intensities of (110) reflection in AA/AB stacking for COF-1, COF-5, COF-6, COF-8 and COF-10.

	COF-1	**COF-5**	**COF-6**	**COF-8**	**COF-10**
Space Group (AA Stacking)	*P*6/*mmm*	*P*6/*mmm*	*P*-6*m*2	*P*-6*m*2	*P*6/*mmm*
I_{110}/I_{100} (AA Stacking)	3.89%	16.5%	2.22%	9.37%	16.4%
Space Group (AB Stacking)	$P6_3/mmc$	$P6_3/mmc$	*P*-6*m*2	*P*-6*m*2	$P6_3/mmc$
I_{110}/I_{100} (AB Stacking)	15.4%	66.0%	8.86%	37.5%	65.5%

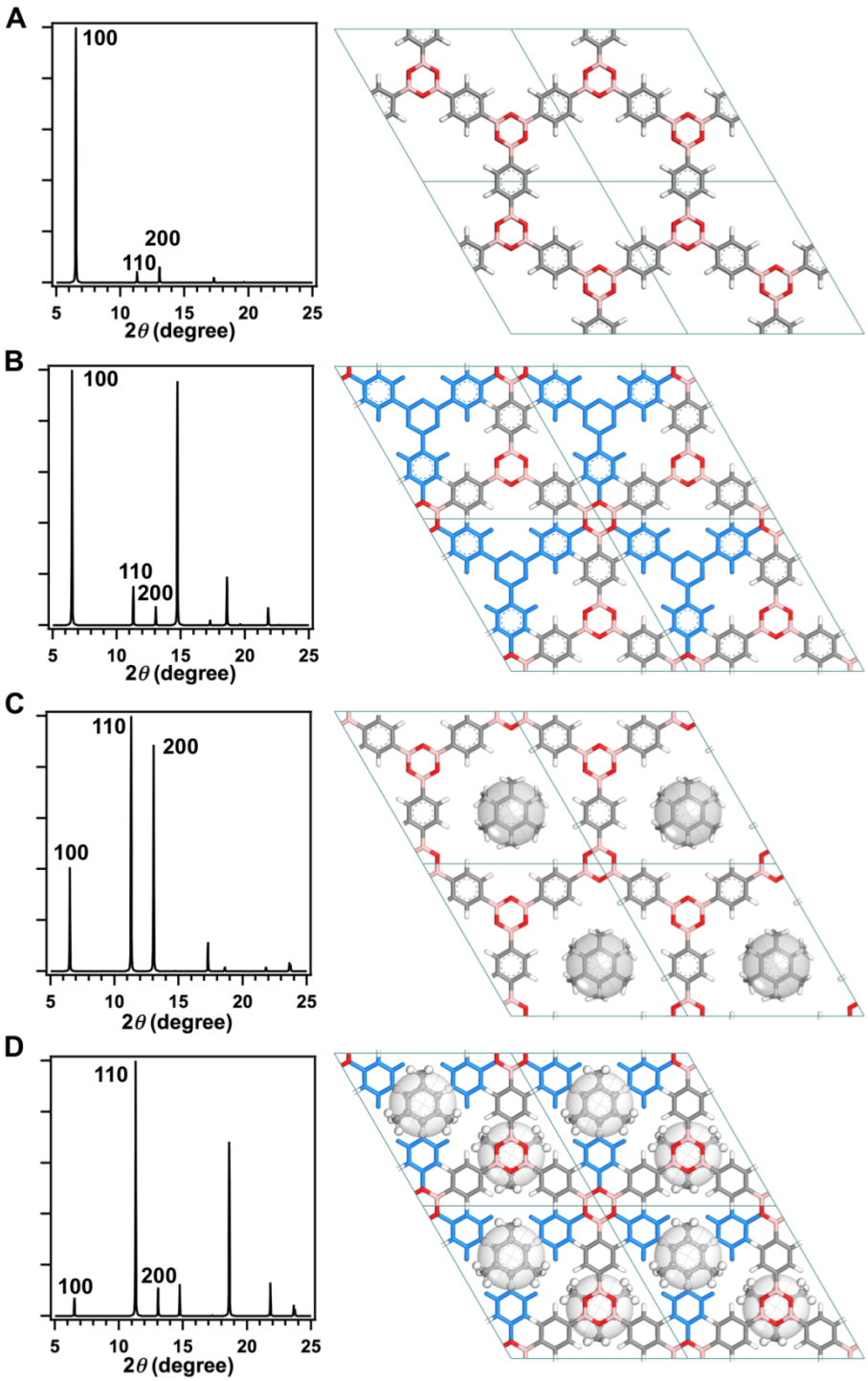

Figure 2. 5. Four types of COF-1 structural models of a) AA stacking without mesitylene molecule in the pore, b) AB stacking without mesitylene molecules in the pores, c) AA stacking with mesitylene molecules in the pores and d) AB stacking with mesitylene molecules in the pores.

For further verification, the author performed molecular dynamics (MD) simulations on AA stacking mode of COF-1 without guest molecules to imitate the lattice deformation in actual circumstance. The result demonstrated that COF-1 tends to adopt slipped AA arrangements with random stacking orientation in adjacent layers, which agrees well with the total energy calculations previously. After that, a snapshot during the stable status was chosen to mimic the partial structure of COF-1 and then different amount of mesitylene molecules was packed into the pores with stochastic configurations in order to evaluate the impact of inserting guest molecules on PXRD spectra. **Figure 2. 6** depicts the change of the simulated PXRD pattern with the apparent density of the mesitylene padding in the pores arising from 0.1 g cm^{-3} to 0.9 g cm^{-3}. There obviously exists a strong correlation between the relative intensity of (110) refection and the amount of the packing mesitylene. In the low loading amount, the XPRD pattern look exactly like the "AA stacking". With more guest molecules are added into the pores, the (110) peak rise gradually together with the decrease of (100) relatively. When the packing amount of mesitylene is close to the maximum value (apparent density approaches 0.864 g cm^{-3}), the PXRD patterns show a perfect match with the experimental COF-1 PXRD before guest removal. The author obtained a substituted structural model replacing AB stacking model for explaining the unique PXRD spectra of COF-1.

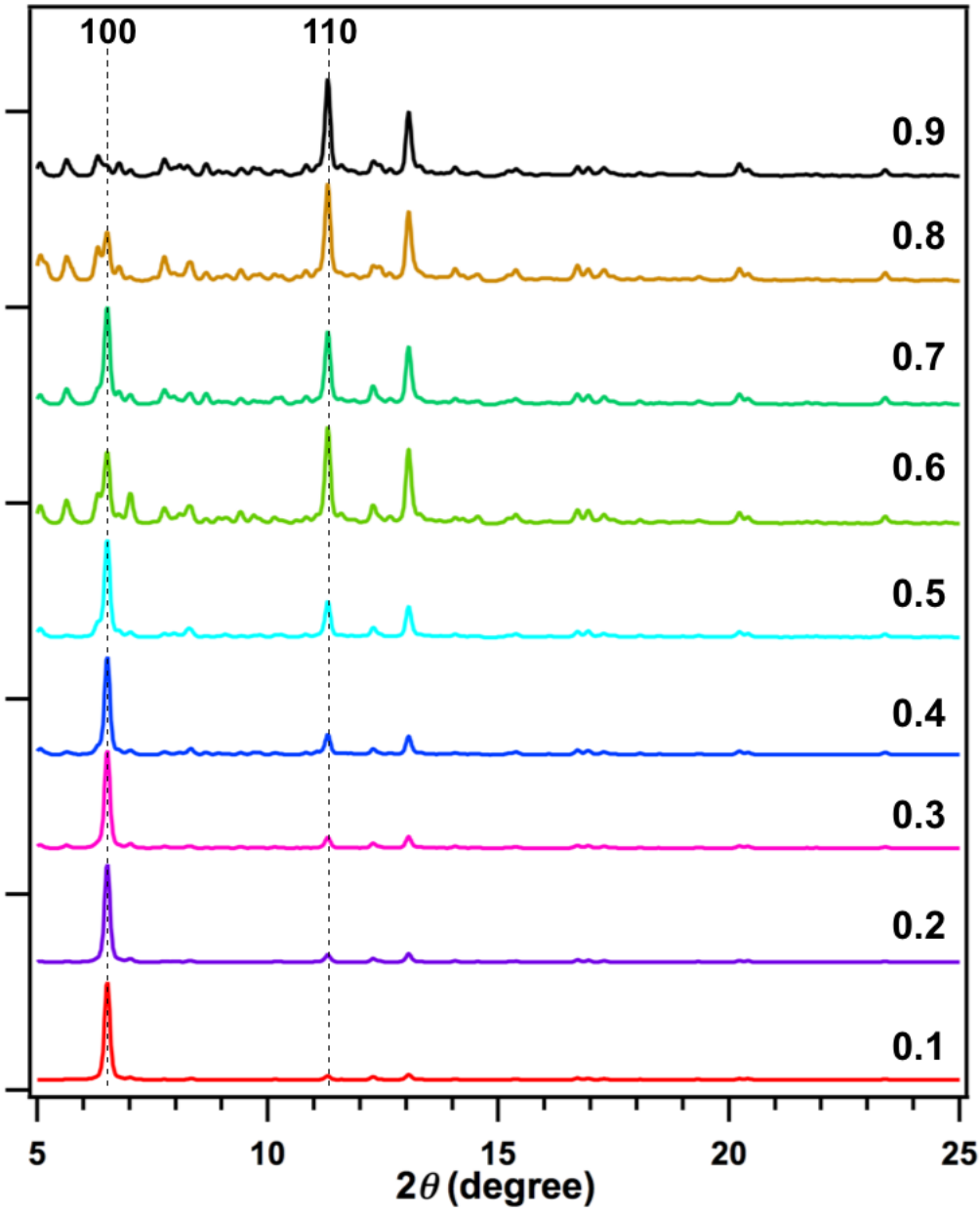

Figure 2. 6. The simulated PXRD patterns of COF-1 with different amount of mesitylene.

However, what is the mechanism behind this magical PXRD spectra changes? To answer this question, the author proposed an approximate model named “centroids model”. For a crystalline solid, the incident X-rays are scattered from lattice planes and the reflected X-rays interfere with each other in forming diffraction patterns. According to the principle of Bragg’s formulation, these lattice planes are constituted with particles that are able to interact with the X-ray. A centroid of a connecter in COF-1 can be treated as such kind of particles because these centroids locates in the special positons with highest symmetry in hexagonal lattice. From a crystallographic point of view, once the actual periodic structure in unit cell was replaced with centroid lattice, the new lattice should inherit all the symmetric relations from the original one and reproduces PXRD pattern with exactly the same peak positions and similar intensity distribution.

When the guest molecules are packed into the pores, the substance added into would change the mass distribution within the unit cell and the consequence varies depending on the difference between the pore sizes and the dimensions of the guest molecules **(Figure 2. 7)**. For COFs with pore size much larger than the guest molecules, guest molecules disperse randomly in the pores without periodicity, which as an amorphous phase, could not interfere with the main specific diffractive peaks but only raise the background noise in PXRD spectra due to the diffuse scattering.

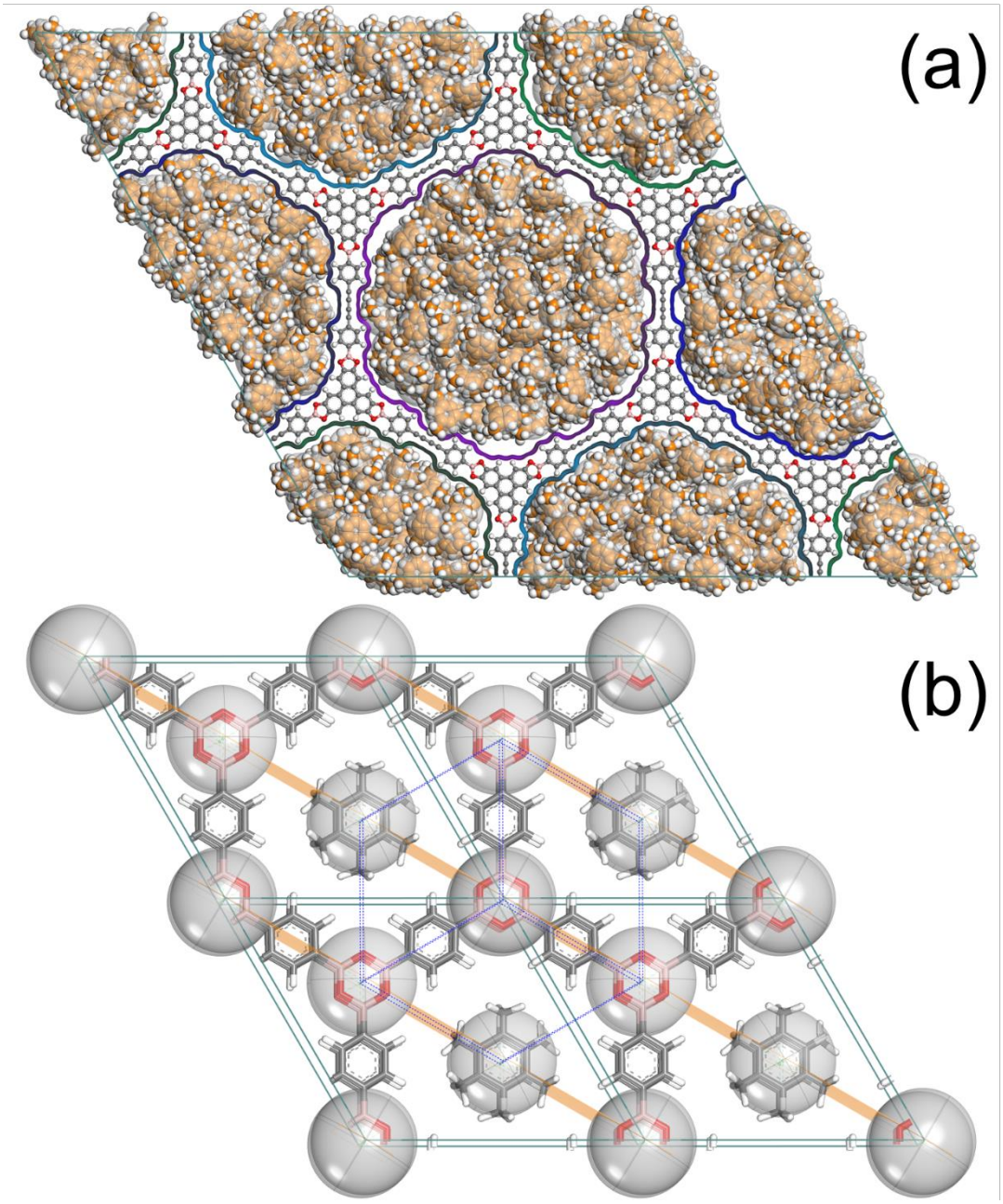

Figure 2. 7. The different influence of added-in guest molecules of a) An example of 2D COF with larger pores and b) COF-1 with a specific pore size.

As for the COF-1, the average pore size is 1.1 nm around and this value is identical with the diameter of mesitylene. The random population of the mesitylene in pores is greatly suppressed in such a small dimension and no matter what configurations mesitylene molecules take, the centroids of the mesitylene will be confined in a small region locating in the geometrical center of the pores where happens to be another special position in hexagonal lattice. The intrinsic symmetry of monolayer is therefore to be altered with the embed mesitylene molecules. The author named this structure with new symmetry as "encapsulated phase". A conventional unit-cell of COF-1 no longer presents the global symmetry of this composite structure and ought to be further subdivided into a "primitive cell" as the blue dot line marked **(Figure 2. 7)**. The (100) spacing of the "primitive cell", which corresponds to the most intense diffraction in new lattice, coincides with the (110) spacing of the conventional cell and the (100) reflection in conventional cell will be decreased due to the structural extinction. Based on measuring the pore volume and the apparent density of COF-1, the maximum loading of mesitylene can be deduced to be at ~23 wt%, equivalent to injecting 1.0 - 1.1 molecules per hexagonal pore in average. It means that almost all the vacancies are taken up by the mesitylene molecules in as-synthesized COF-1 and the (110) reflection shall to be the strongest signal in PXRD spectra exactly as observed in PXRD experiment. During the guest

removal, the proportion of “encapsulated phase” in the whole sample is reduced together with the relative intensity of (110) reflection declines. After most of the guest molecules are expelled out of the pores, the diffractions from intrinsic framework of COF-1 occupy the dominant position again and the activated COF-1 sample, consequently, shows a typical “AA stacking” PXRD pattern. This is the essence of how the unique PXRD pattern of as-synthesized COF-1 forms and vanishes, which dramatically depicts a double symbolic meaning of the porosity and the symmetry emerging in 2D COFs.

The author would like to emphasize that the above explanation is not limited to COF-1. Any COFs with a proper pore size matching with the guest molecules have a possibility to exhibit an abnormal PXRD pattern like COF-1, in spite of their topologies and styles of connections. The author expects that a similar phenomenon can be observed for other COFs with small pores size such as COF-6 and COF-LZU1, an imine-linked COF, by choosing the experiment conditions deliberately.

2. 4 Conclusion

In this chapter, the author studied the changes of PXRD pattern of COF-1 through structural simulations using different interlayer offsets and integrating mesitylene guest molecules into the nanochannels. The present results unambiguously demonstrate that the layered structure of COFs is highly dependent on the skeletons that directly provide the π-π forces in directing the framework formation, whereas solvents and/or guest molecules are fully involved in the crystallization process. Not only the stacking mode but also the PXRD pattern of the resulting COF samples is highly dependent on the solvent or guest molecules involved. The molecular dynamic strategy provides a new tool to resolve the lattice structures of COFs. Our results also imply that the integration of 'designed guest' with suitable size to fill the channel space may help to form well-defined crystals of COFs and leads to unambiguous resolution of crystal structures of COF materials.

2. 5 References

1. X. Feng, X. Ding and D. Jiang, *Chem. Soc. Rev.*, 2012, **41**, 6010.
2. S.-Y. Ding and W. Wang, *Chem. Soc. Rev.*, 2013, **42**, 548.
3. A. P. Cote´, A. I. Benin, N. W. Ockwig, M. O' Keeffe, A. J. Matzger and O. M. Yaghi, *Science*, 2005, **310**, 1166.
4. X. Chen, M. Addicoat, E. Jin, L. Zhai, H. Xu, N. Huang, Z. Guo, L. Liu, S. Irle and D. Jiang, *J. Am. Chem. Soc.*, 2015, **137**, 3241.
5. C. R. DeBlase, K. E. Silberstein, T.-T. Truong, H. D. Abruna and W. R. Dichtel, *J. Am. Chem. Soc.*, 2013, **135**, 16821.
6. H.-S. Cho. H. Deng, K. Miyazaka, Z. Dong, M. Cho, A. V. Neimark, J. Ku, O. M. Yaghi and O. Terasaki, *Nature*, 2015, **572**, 503.
7. A. P. Cote´, H. M. El-Kaderi, H. Furukawa, J. R. Hunt and O. M. Yaghi, *J. Am. Chem. Soc*. 2007, **129**, 12914.
8. S. Kandambeth, D. B. Shinde, M. K. Panda, B. Lukose, T. Heine and R. Banerjee, *Angew. Chem., Int. Ed.*, 2013, **52**, 13052.
9. L. M. Lanni, R. W. Tilford, M. Bharathy and J. J. Lavigne, *J. Am. Chem. Soc.*, 2011, **133**, 13975.
10. P. Kuhn, M. Antonietti and A. Thomas, *Angew. Chem., Int. Ed.*, 2008, **47**, 3450.
11. H. Xu, X. Chen, J. Gao, J. Lin, M. Addicoat, S. Irle and D. Jiang, *Chem. Commun.*, 2014, **50**, 1292.

12. D. B. Shinde, S. Kandambeth, P. Pachfule, R. R. Kumar and R. Banerjee, *Chem. Commun.*, 2015, **51**, 310.

13. P. Pachfule, M. K. Panda, S. Kandambeth, S. M. Shivaprasad, D. Dı´az Dı´az and R. Banerjee, *J. Mater. Chem. A*, 2014, **2,** 7944.

14. Q. Fang, Z. Zhuang, S. Gu, R. B. Kaspar, J. Zheng, J. Wang, S. Qiu and Y. Yan, *Nat. Commun.*, 2014, **5**, 4503.

15. S. Y. Ding, J. Gao, Q. Wang, Y. Zhang, W. Song, C. Su and W. Wang, *J. Am. Chem. Soc.*, 2011, **133**, 19816.

16. B. Lukose, A. Kuc and T. Heine, *Chem. – Eur. J.*, 2011, **17**, 2388.

17. B. Lukose, A. Kuc, J. Frenzel and T. Heine, Beilstein J. *Nanotechnol.*, 2010**, 1**, 60.

18. W. Zhou, H. Wu and T. Yildirim, *Chem. Phys. Lett*., 2010, **499**, 103.

19. B. T. Koo, W. R. Dichtel and P. Clancy, *J. Mater. Chem.*, 2012, **22**, 17460.

20. Y. Du, D. Calabro, B. Wooler, Q. Li, S. Cundy, P. Kamakoti, D. Colmyer, K. Mao and P. Ravikovitch, *J. Phys. Chem. C.*, 2014, **118,** 399.

21. Materials Studio Release Notes v.4.4 (Accelrys Software, 2008).

22. S. L Mayo, B. D. Olafson and W. A. Goddard III, *J. Phys. Chem.*. 1990, **94**, 8897.

23. T. Darden, D. York and L. Pedersen, *J. Chem. Phys.*, 1993, **98**,

10089.

24. M. L. Connolly, *J. Appl. Crystal.*, 1983, **16**, 548.

Chapter 3

The Twisted Stacking Structure of Two Dimensional Covalent Organic Frameworks

Abstract

In this chapter, the author proposed a hypothesis model for π-stack ordering based on the relative rotation of the adjacent 2D COF layers. The modeling method for the twisted stacking structure that is formed with relative rotation was deduced. The differences on PXRD pattern and other properties between the twisted stacking structure and the classical 2D COF structures are discussed.

3. 1 Introduction

In the previous chapter, the author performed Molecular Dynamics (MD) simulations on AA stacking mode of COF-1 to investigate the interlayer deformation. Although the simulated PXRD pattern matched with the experiment data very well in peak positions, the asymmetric peak shape in experimental pattern implies that there still exists significant differences between the models and the actual structures of 2D COFs[1)].

Up to now, all the studies about the stacking arrangements are based on an assumption that the deformation of 2D COFs only comes from the interlayer shifting between two adjacent COF planes[2-13)]. By applying part of symmetry operations attributed to the space group of unit cell, the two adjacent COF planes are always able to coincide with each other. In this regulation, all the staking arrangements are the variants of slipped AA-stacking. However, if one layer takes an in-plane rotation relative to the other one, the symmetry of the two-layer system will be completely changed. In this chapter, the author presented a discussion about the potential of twisted stacking model of 2D COFs and their properties.

3. 2 Modeling Method

The principle of twisted stacking was well developed in some research about the graphene[14-18]. Given the fact that most of 2D COFs are belong to hexagonal lattice, the author took honeycomb topology graph to simplify the hexagonal COF unit cells. Please note that all the 2D COFs with hexagonal, tetragonal and trigonal lattices can have a chance to form twisted stacking structure.

Figure 3. 1 is a schematic of the twisted stacking structure for hexagonal lattice. The primitive lattice vectors for the original layer are defined as $\boldsymbol{a}_1 = a\ (\sqrt{3}/2,\ 1/2)$ and $\boldsymbol{a}_2 = a\ (\sqrt{3}/2,\ -1/2)$ and $a = |\boldsymbol{a}_1| = |\boldsymbol{a}_2|$ is the lattice constant of original unit cell, which is $\sqrt{3}$ times of hexagon edges. The two layers have two vectors $\boldsymbol{V}_1$ and $\boldsymbol{V}_2$, $\boldsymbol{V}_1 = m\boldsymbol{a}_1 + n\boldsymbol{a}_2$; $\boldsymbol{V}_2 = m\boldsymbol{a}_2 + n\boldsymbol{a}_1$ where n and m are integers ($0 < m < n$). $\boldsymbol{V}_1$ and $\boldsymbol{V}_2$ have different direction. Rotate any vector based on one sublattice site in a layer to make $\boldsymbol{V}_1$ and $\boldsymbol{V}_2$ coincide. The rotation angle θ is related to (m, n) with:

$$\cos\theta = \frac{1}{2}\frac{m^2+4mn+n^2}{m^2+mn+n^2} \qquad \textbf{(3.1)}$$

The lattice vectors of the superlattice unit cell are thus given:

$$\boldsymbol{T}_1 = \boldsymbol{V}_2 = n\boldsymbol{a}_1 + m\boldsymbol{a}_2;\ \boldsymbol{T}_2 = -m\boldsymbol{a}_1 + (m+n)\,\boldsymbol{a}_2$$

The lattice constant $\boldsymbol{L}$ is

$$L = a\sqrt{m^2+mn+n^2} = \frac{a|m-n|}{2\sin(\theta/2)} \qquad \textbf{(3.2)}$$

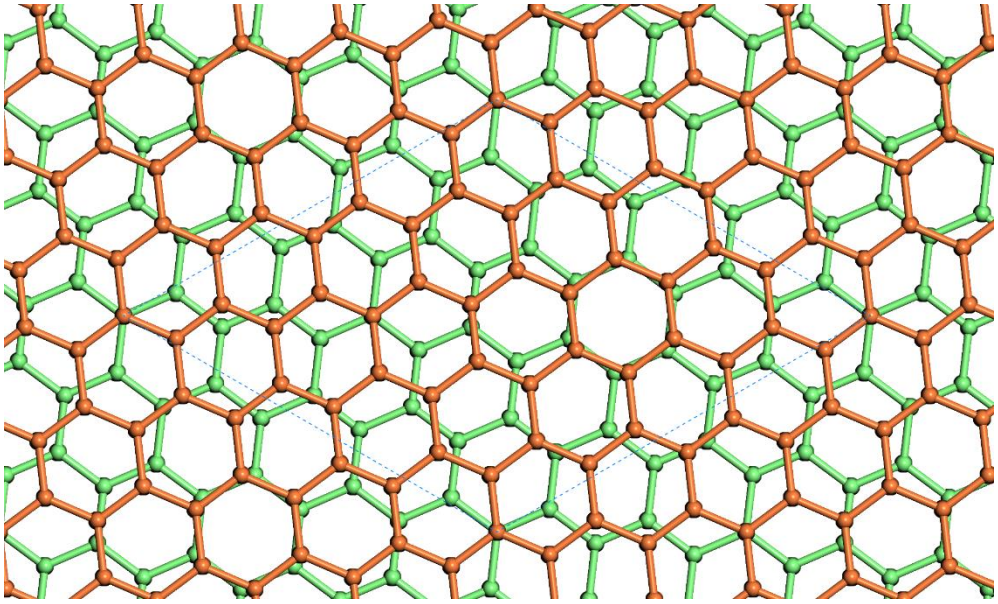

Figure 3. 1. Illustration diagram for the concept of twisted stacking structure.

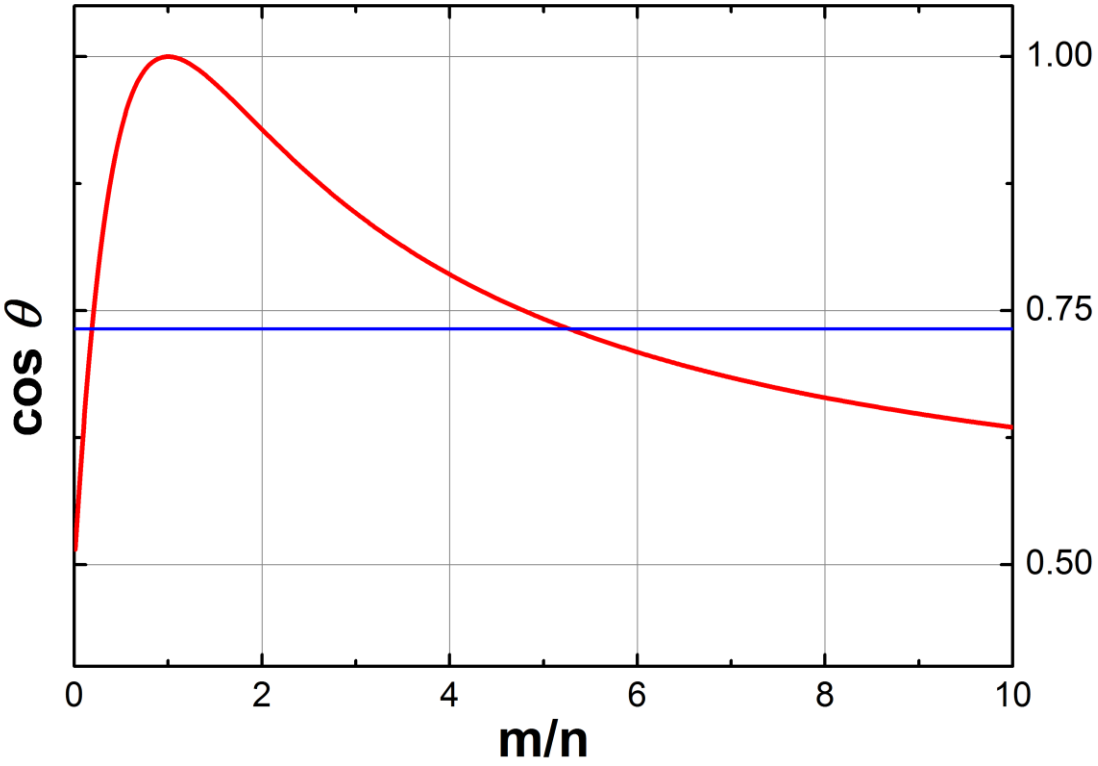

Figure 3. 2. The dependence between (m, n) and rotation angle θ.

3. 3 Results and Discussions

The repeat period of the rotation angle θ is 120°, When the rotations θ = 0 and 60°, the stacking order is AA and AB stacking, respectively. 60°- θ is equivalent to - θ followed by a relative translation and θ and - θ are mirror images sharing equivalent band structures. It's note that the value of the rotation angle θ is continuous, but not every value of θ can find a pair of integers (*m, n*) to set up a super lattice that can satisfy the two layers match with each layer, for example, when θ = 30°. In this case, a series of integers (*m, n*) can be selected to approximate the value of cosθ, and the lattice constant *L* is variable **(Figure 3. 2)**.

The concept of twist angle θ adds a new degree of freedom to the 2D COF systems and provides a possibility for stacking arrangements. By adding a twist angle θ between the layers, the AA or AB-staking modes disappear and a super lattice structure is formed, generating several θ-dependent phenomena that cannot occur in the AA or AB-stacking system. In this chapter, the author selected COF-1 structure to demonstrate the effects of twisted stacking on the structure and properties of 2D COFs.

Because the overall scale of the super lattice increases in square with the value of *(m, n),* the author adopts (2, 1) and (3, 1) to build the super lattice of twisted stacking COF-1 for a comparison.

Figure 3. 3 shows the 2 × 2 super cell of the twisted stacking COF-1 in (2, 1) and (3, 1), the author named as COF-1-(2, 1) and COF-1-(3, 1). The most obvious difference comparing with the classical stacking arrangement modes such as AA-stacking, AB-stacking and slipped-AA stacking is the offset distances and the offset directions for the different topical parts of COF skeleton. In some parts, the stacking order is similar to the AA-stacking while in some other parts the stacking order is close to the AB-stacking, but the homogeneous status of the structure arrangements is broken. In a word, the AA-stacking, AB-stacking and slipped-AA stacking can coexist in one 2D COF. This result offers a new approach to the structural understanding of 2D COFs.

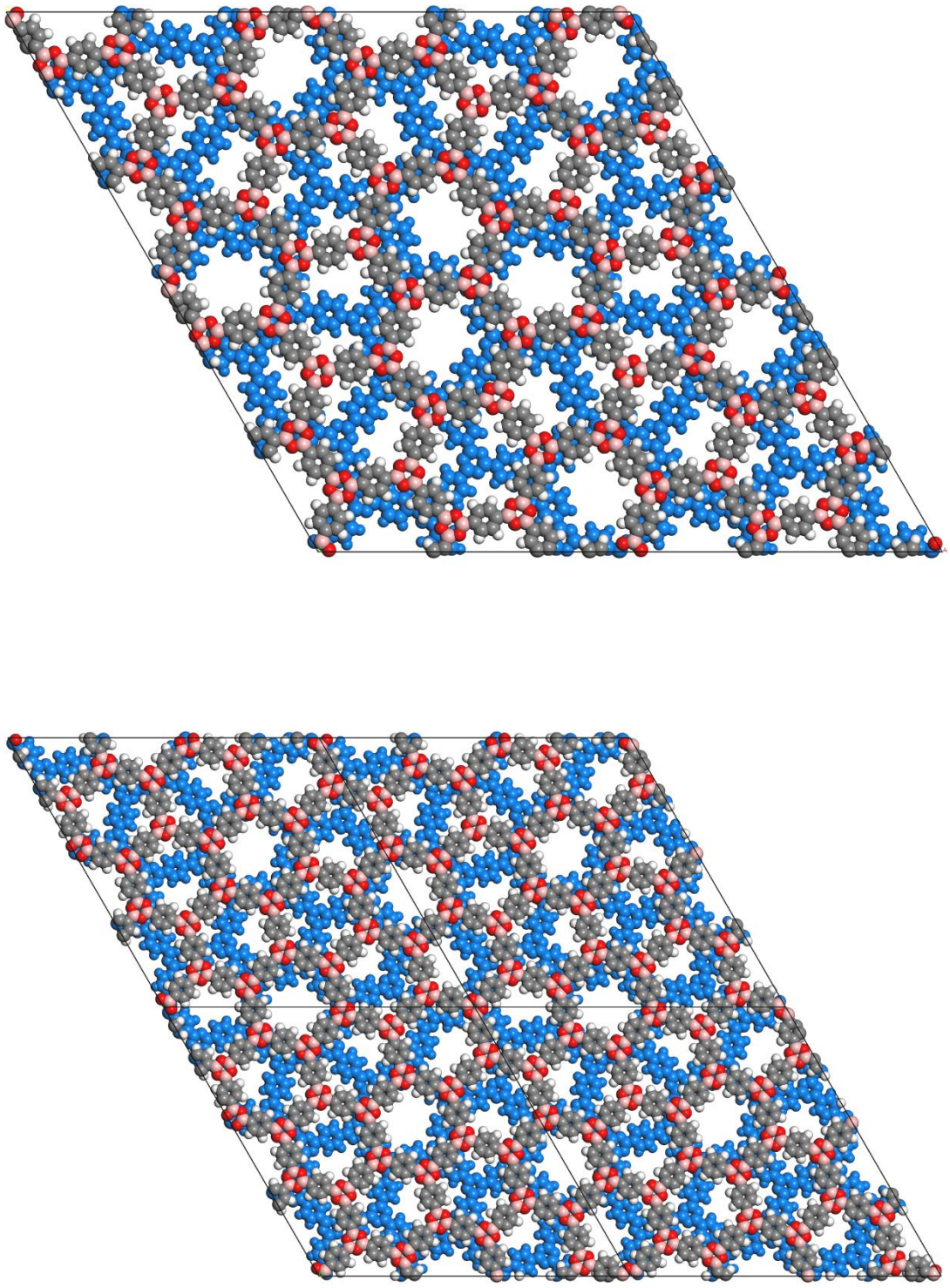

Figure 3. 3. The simulated models of COF-1-(2, 1) (upper) and COF-1-(3, 1) (lower).

The most critical influence that the concept of twisted stacking brought up, is the reconsideration of the reliability of the Powder X-ray Diffraction technique on determining the crystalline structure of 2D COFs.

PXRD technique is the foundation for the research of COF materials. All the crystalline structures of 2D COF are solved based on the analysis of PXRD spectra. Moreover, the comparison between the simulated XPRD patterns and the experimental PXRD patterns for determining the stacking arrangement of 2D COFs is a general procedure in every published literature on COFs field. However, in a twisted stacking structure of 2D COFs, AA-stacking, AB-stacking and slipped-AA stacking are coexisted, which make the necessity of such comparison extremely susceptible.

The most important thing is the relative rotation between the adjacent layers do not changes the position of the main diffraction peaks. **Figure 3. 4** depicts a comparison of simulated PXRD patterns between the native lattice of COF-1, COF-1-(2, 1) and COF-1-(3, 1). The main diffraction marked out in diagram is exactly the same both in the position and in the relative intensities. However, some other small peaks such as that at 15° appeared in the simulations of COF-1-(2, 1) and COF-1-(3, 1) but not for COF-1. This phenomenon can be explained with the basic principle of PXRD technique.

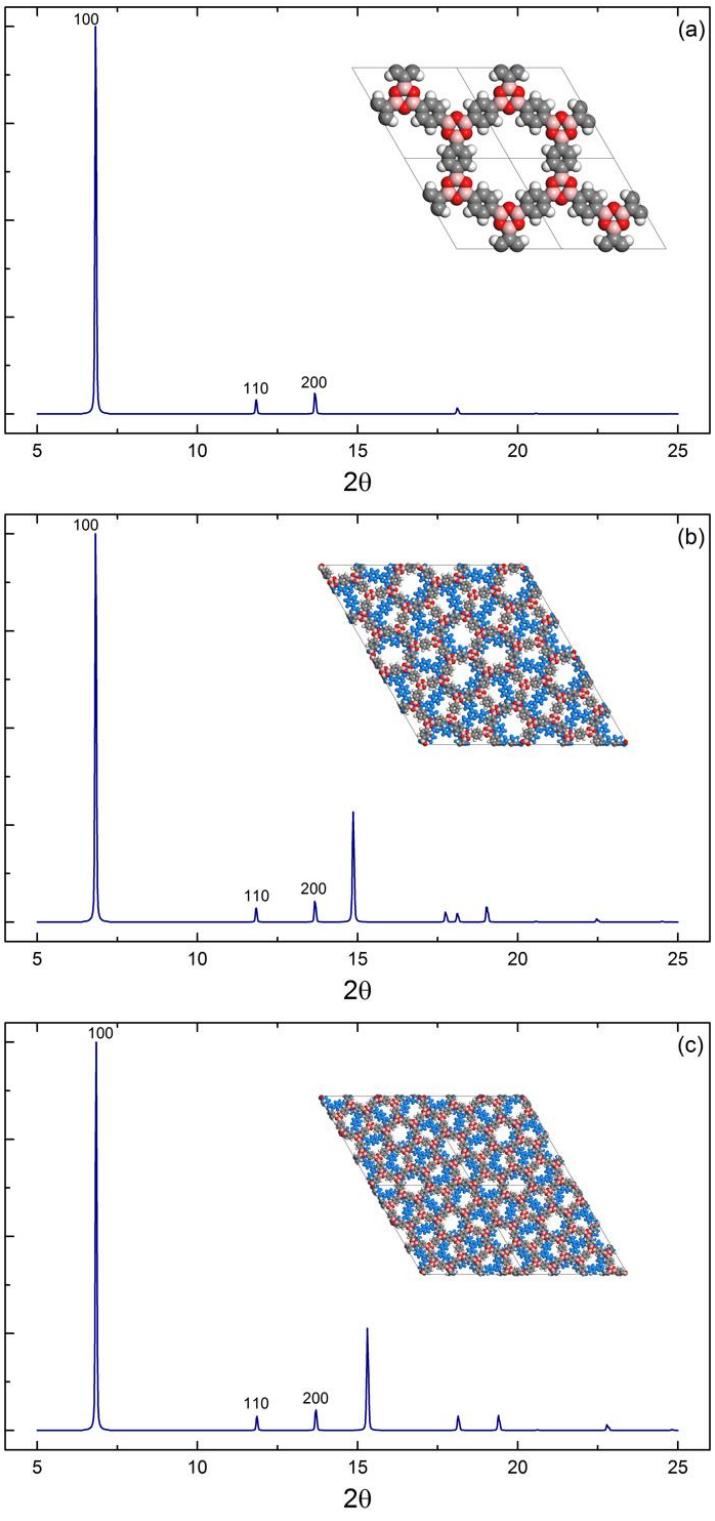

Figure 3. 4. The simulated PXRD pattern of a) COF-1, b) COF-1-(2, 1) and c) COF-1-(3, 1).

The twisted stacking model gives rise to a new possibility of COF structural models by selecting different rotation angles. In each given rotation angles, the interlayer offset can also exist. Three different high symmetry position of stacking position were found, whose space group are *P*-62*c, P*6*/mcc* and *CCCm.* The three positions are similar to the AA-stacking and AB-stacking in the traditional stacking models and their space group remains even in different *(m, n)* value.

Unfortunately, the direct experimental evidences of the twisted stacking COF structure have not been observed. In author's prediction, the existence of twisted stacking in 2D COFs can change the pore distribution and consequently, some clues may be gained upon gas adsorption analysis of different 2D COFs.

3. 4 Conclusion

In this chapter, the author discussed the possibility of twisted stacking model in 2D COFs. By analyzing the twisted stacking models in different rotation angles, the author shows that the relative rotation between adjacent COF layers causes less effect on PXRD pattern. This result would add new aspects to the crystalline structure of 2D COFs.

3. 5 References

1) J. R. Long and O. M. Yaghi, *Chem. Soc. Rev.*, 2009, **38**, 1213.

2) D. J. Tranchemontagne, J. L. Mendoza-Corte´ s, M. O'Keeffe and O. M. Yaghi, *Chem. Soc. Rev.*, 2009, **38**, 1257.

3) E. L. Spitler, B. T. Koo, J. L. Novotney, J. W. Colson, F. J. Uribe-Romo, G. D. Gutierrez, P. Clancy and W. R. Dichtel, *J. Am. Chem. Soc.*, 2011, **133**, 19416.

4) E. L. Spitler and W. R. Dichtel, *Nat. Chem.*, 2010, **2**, 672.

5) E. L. Spitler, J. W. Colson, F. J. Uribe-Romo, A. R. Woll, M. R. Giovino, A. Saldivar and W. R. Dichtel, *Angew. Chem., Int. Ed.*, 2012, **51**, 2623.

6) S. Wan, F. Gandara, A. Asano, H. Furukawa, A. Saeki, S. K. Dey, L. Liao, M. W. Ambrogio, Y. Y. Botros, X. Duan, S. Seki, J. F. Stoddart and O. M. Yaghi, *Chem. Mater.*, 2011, **23**, 4094.

7) S. Kandambeth, A. Mallick, B. Lukose, M. V. Mane, T. Heine and R. Banerjee, *J. Am. Chem. Soc.*, 2012, **134**, 19524.

8) B. P. Biswal, S. Chandra, S. Kandambeth, B. Lukose, T. Heine and R. Banerjee, *J. Am. Chem. Soc*., 2013, **135**, 5328.

9) F. J. Uribe-Romo, C. J. Doonan, H. Furukawa, K. Oisaki and O. M. Yaghi, *J. Am. Chem. Soc.*, 2011, **133**, 11478.

10) X. Feng, L. Liu, Y. Honsho, A. Saeki, S. Seki, S. Irle, Y. Dong, A. Nagai and D. Jiang, *Angew. Chem., Int. Ed.*, 2012, **51**, 2618.

11) X. Feng, L. Chen, Y. Honsho, O. Saengsawang, L. Liu, L. Wang, A. Saeki, S. Irle, S. Seki, Y. Dong and D. Jiang, *Adv. Mater.*, 2012, **24**, 3026.

12) S. Jin, X. Ding, X. Feng, M. Supur, K. Furukawa, S. Takahashi, M. Addicoat, M. E. El-Khouly, T. Nakamura, S. Irle, S. Fukuzumi, A. Nagai and D. Jiang, *Angew. Chem., Int. Ed.*, 2013, **52**, 2017.

13) M. Dogru, M. Handloser, F. Auras, T. Kunz, D. Medina, A. Hartschuh, P. Knochel and T. Bein, *Angew. Chem. Int. Ed.*, 2013, **125**, 2992.

14) J. M. B. Lopes dos Santos, N. M. R. Peres and A. H. Castro Neto, *Phys. Rev. Lett.,* 2007, **99**, 256802.

15) J. Mele, *Phys. Rev. B.,* 2010*,* **81**, 161405.

16) S. Shallcross, S. Sharma, E. Kandelaki and O. A. Pankratov, *Phys. Rev. B.,* 2010, **81**, 165105.

17) G. T. Laissardiere, D. Mayou and L. Magaud, *Nano Lett.*, 2010, **10,** 804.

18) E. S. Morell, J. D. Correa, P. Vargas, M. Pacheco and Z. Barticevic, *Phys. Rev. B.,* 2010, **82**, 121407.

Chapter 4

Observation and Curvature Model of Hollow Spherical Structures of Covalent Organic Frameworks

Abstract

In this chapter, the author reported that an imine-linked COF with triphenylbenzene vertices and phenyl edges (TPB-DMTP-COF) under certain conditions formed hollow spherical nanoparticles. By combining SEM, TEM and polarizing microscope analysis techniques, the author further verified the existence of spherical particles with sizes ranging from nanometer scale to microscopic scale. These spherical particles consist of multiple curved COFs layers with a hollow central space. The author proposed a curvature model to elucidate the origin of these hollow spherical particles, which may complement the model of 2D COF crystalline structures.

4. 1 Introduction

Xu *et al.* reported a successful synthesis of a 2D COF that combines outstanding stability with high crystallinity and porosity. This COF, i.e., TPB-DMTP-COF (TPB, triphenylbenzene; DMTP, dimethoxyterephthaldehyde), possesses C_3-symmetric TPB vertices and electron-donating methoxy-substituted C_2-symmetric phenyl edges (**Figure 4. 1**)[1]. The COF has a Brunauer–Emmett–Teller (BET) surface area of 2,105 $m^2\ g^{-1}$, which approaches the theoretical boundary of the maximum surface area (2100 - 2200 $m^2\ g^{-1}$). The full-width at half-maximum (FWHM) values of PXRD peaks is smaller than the empirical value, which suggests that TPB-DMTP-COF samples has a high crystallinity comparing with the other 2D COFs[2-12]. The COF sample is thermally stable up to 400 °C under nitrogen and retains its crystallinity and porosity even after treatments in boiling water, strong acids and strong bases. The BET surface areas were 2,081, 2,074 and 2,020 $m^2\ g^{-1}$ for the COF samples treated for one week in boiling water, strong acid and strong base, respectively; these values are very close to that of the as-synthesized COF. In contrast to TPB-DMTP-COF, TPB-TP-COF without methoxy groups on the walls exhibited a low chemical stability, which is indicated by the more-significant weight loss after treatment in acid, base or boiling water. The outstanding stability and crystallinity of TPB-DMTP-COF inspired the author to investigate

the essence of 2D COF crystallinity. In this chapter, the author focused on elucidation of the high-order structures of TPB-DMTP-COF especially the spherical form of this COF.

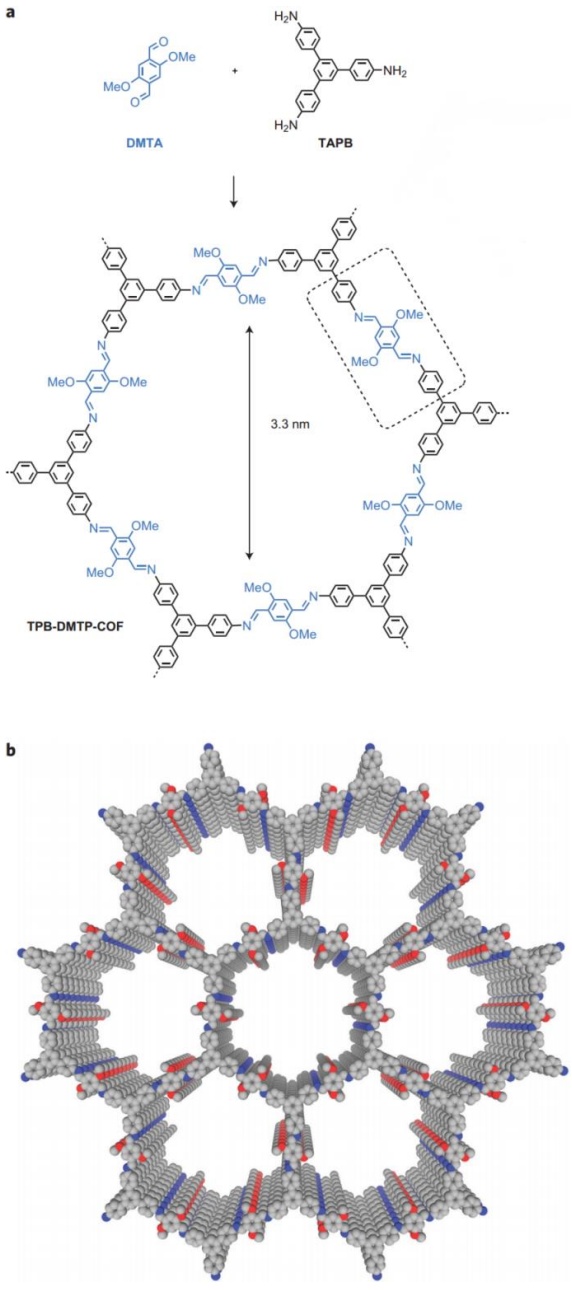

Figure 4. 1. a) Synthesis of TPB-DMTP-COF through the reaction of DMTA (blue) with TAPB (black). b) Graphic view of TPB-DMTP-COF (red, O; blue, N; grey, C; hydrogen is omitted for clarity).

4.2 Experimental

Powder X-ray diffraction (PXRD) data were recorded on a Rigaku model RINT Ultima III diffractometer by depositing powder on glass substrate, from 2θ = 1.5° up to 60° with 0.02° increment. The XRD pattern simulation was performed in a software package for crystal determination from PXRD pattern, implemented in MS modeling version 4.4 (Accelrys Inc.) [13]. Pawley refinement was performed to optimize the lattice parameters iteratively until the R_P and R_{WP} values converge. The pseudo-Voigt profile function was used for whole profile fitting and Berrar-Baldinozzi function was used for asymmetry correction during the refinement processes.

All the modeling work was conducted in the platform of Materials Studio 4.4. The models of COF structures were optimized by using the density functional tight binding (DFTB) method with Lennard-Jones (LJ) dispersion. The calculations were carried out with the DFTB+ program package version 1.2[14]. DFTB is an approximate density functional theory method based on the tight binding approach and utilizes an optimized minimal LCAO Slater-type all-valence basis set in combination with a two-center approximation for Hamiltonian matrix elements. The Coulombic interaction between partial atomic charges was determined using the self-consistent charge (SCC) formalism. Lennard-Jones type dispersion was employed in all calculations to describe van der Waals

(vdW) and π-stacking interactions. The lattice dimensions were optimized simultaneously with the geometry. Standard DFTB parameters for X–Y element. pair (X, Y = C, O, H and N) interactions were employed from the mio-0-1 set[15]. The accessible surface areas were calculated from the Monte Carlo integration technique using a nitrogen-size probe molecule (diameter = 3.68 Å) roll over the framework surface with a grid interval of 0.25 Å[16].

The TPB-DMTP-COF samples were synthesized following the procedures as reported in the literature[1]. The final product is yellow powder with bright fluorescence in UV light. The COF samples were soaked in *N*-methylpyrrolidone (NMP), *N*,*N*-dimethylacetamide (DMAc), g-butyrolactone (GBL) and 1, 3-dimethyl-2-imidazdidione (DMEU), respectively, and then kept in microwave reactor at 100 °C, overnight. The resulting COF samples were sonicated for one hour and centrifuged. The top half of the dispersions was collected for examination using SEM, TEM and PLM.

4.3 Results and Discussion

The PXRD pattern of TPB-DMTP-COF exhibited six prominent diffraction peaks, with the most intensive one at 2.76° (FWHM = 0.39°) and the five other peaks at 4.82, 5.60, 7.42, 9.70 and 25.2°; these peaks were assigned to the (100), (110), (200), (210), (220) and (001) facets, respectively (**Figure 4. 2**). The (100) signal is sharp compared with that of TPB-TP-COF under the same PXRD experimental conditions. Another feature is that the PXRD pattern contains more peaks than those for other imine-linked COFs. The (100) signal is sharper compared with that of TPB-TP-COF under the same PXRD experimental conditions and the overall PXRD pattern contains more peaks than those for other imine-linked COFs. Simulated PXRD pattern of the AA stacking mode matched the experimental peak positions and intensities well. The final R_P and R_{WP} values were 2.02 % and 4.37 %. The analysis results on PXRD spectra show indirect evidence that the sample of TPB-DMTP-COF is crystalline in decent.

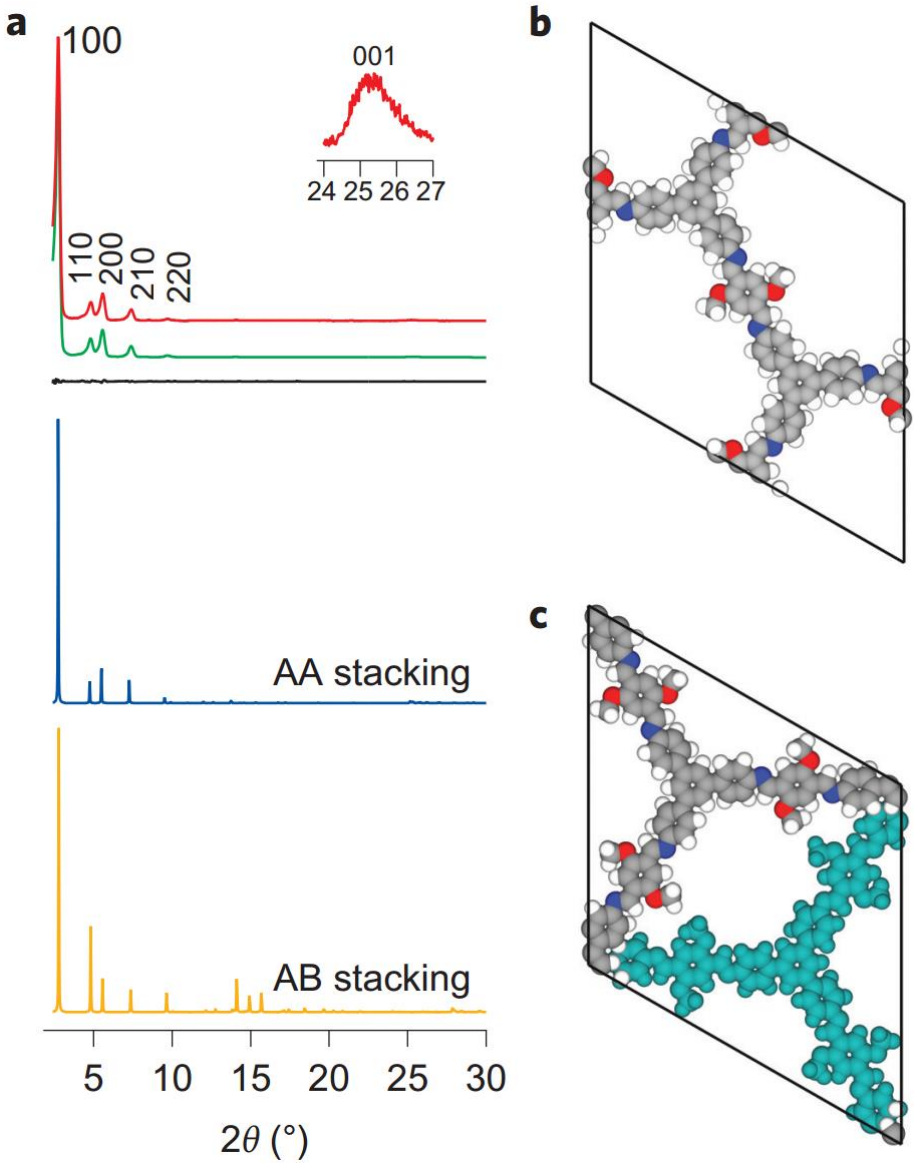

Figure 4. 2. a) PXRD profiles of TPB-DMTP-COF. Experimentally observed (red), Pawley refined (green) and difference (black), simulated using the AA stacking mode (blue) and the staggered AB stacking mode (orange). b) Unit cell of the AA stacking mode. c) Unit cell of the AB stacking mode.

A density-functional tight-binding method, which included a Lennard–Jones dispersion, was used to simulate the optimum structures of TPB-DMTP-COF and investigate the crystal stacking energy of TPB-DMTP-COF and, TPB-TP-COF (TP, terephthaldehyde), that lacks methoxy groups. Using the optimal monolayer structure, AA and staggered AB stacking modes were generated and optimized. In the stacked frameworks, TPB-DMTP-COF adopts the AA stacking mode of a space group of *P6* with $a = b = 37.2718$ Å, interlayer distance (c) of 3.5215 Å. TPB-DMTP COF has a crystal stacking energy of 106.862 kcal mol^{-1} **(Table 4. 1)**, which is not much higher than that of TPB-TP-COF (94.084 kcal mol^{-1}). The comparation based on the stacking energies implies that the planar structure of TPB-DMTP-COF cannot effectively explain the origin of its high stability and crystallinity.

Table 4. 1. Calculated crystal stacking energy for TPB-TP-COF, TPB-DHTP-COF and TPB-DMTP-COF.

COFs	E_{stack}	E_L	E_e
TPB-TP-COF	94.084	97.632	3.548
TPB-DHTP-COF	102.597	102.639	0.042
TPB-DMTP-COF	106.862	107.129	0.267

E_{stack} = crystal stacking energy, E_L = London dispersion energy, E_e = electronic energy. Energies are per unit cell and are given in kcal mol^{-1}.

The atomistic coordinates of for the AA-stacking mode of TPB-DMTP-COF optimized by using DFTB+ method are also attached for further verification by other researchers **(Table 4. 2)**.

Table 4. 2. Atomistic coordinates for the AA-stacking mode of TPB-DMTP-COF optimized by using DFTB+ method (space group *P*6, $a = b = 37.2718$ Å, $c = 3.5215$ Å, $\alpha = \beta = 90°$ and $\gamma = 120°$).

Atom	*x/a*	*y/b*	*z/c*
C1	0.28981	0.64218	0.50948
C2	0.31459	0.62381	0.50941
C3	0.24366	0.61623	0.51129
C4	0.36807	0.58669	0.38149
C5	0.39171	0.56757	0.38659
C6	0.43264	0.5889	0.52061
C7	0.44902	0.63002	0.64034
C8	0.42488	0.64857	0.64092
N9	0.45939	0.5724	0.51985
C10	0.44488	0.53315	0.57564
C11	0.47293	0.51623	0.56578
C12	0.45731	0.47302	0.55581
C13	0.48409	0.45714	0.56395
O14	0.41445	0.44831	0.5392
C15	0.6025	0.59337	0.4059
H16	0.29983	0.59004	0.50963
H17	0.33674	0.5694	0.26378
H18	0.37848	0.53614	0.27277
H19	0.4808	0.647	0.74741
H20	0.43845	0.68015	0.75146
H21	0.41157	0.51089	0.6386
H22	0.47267	0.42382	0.57064
H23	0.58332	0.59569	0.18083
H24	0.63352	0.6031	0.2931
H25	0.60577	0.61504	0.63593

Transmission electron microscopy (TEM) technique is widely considered as a powerful skill that can directly determine the formation of 2D COF structure. Once the lattice structure of 2D COF is found in TEM images, the distance of the patterns is confirmed, and close to the layer distance or theoretical pore sizes. It is commonly believed that the COFs are successfully synthesized in that case. Hence, the author presumed that the crystalline degree of COF sample synthesized in experiment can been roughly estimated by investigating the proportion of the lattice structure taken up the whole specimen in TEM scope.

However, after thoroughly checking a plenty of TEM images taken form TPB-DMTP-COF, the author observed that the situation is much more complicated than expected. Due to the ultrahigh resolution of TEM microscopy, the field of view is quite narrow, during which the layer structure and the hexagonal pores are sharply observed in TEM images. In this situation, the lattice structure of COFs can be located by deliberately choosing the designated magnified zone. However, the TEM images captured in this mode have a strong tendency of anthropic factors and lack statistical representative of the morphology distribution of the whole COF sample. In author's comprehension, high magnitude TEM images have a possibility of neglecting the structural information in detail. Therefore, all the analysis in this chapter is based both on high and middle magnitudes to avoid the suspicion of selective sampling.

By screening the TEM images captured from different COF samples, the author found that there exist two kinds of morphology with compatible abundance in TPB-DMTP-COF. One kind is the ordinary lamellar morphology **(Figure 4. 3)**. In the lamellar morphology, the COF particles show planner structure and the hexagonal lattice can be observed from top view in high resolution. Besides lamellar morphology, the author discovered another morphology with surface structures **(Figure 4. 4)**. In lower magnitude, this morphology appears as aggregations of nano particles with diameters no larger than 100 nm. In higher magnitude, the structural details of individual particle can be clearly revealed. Different from the traditional lamellar morphology of 2D COFs, TPB-DMTP-COF nano particles are constituted with smooth, continuous surfaces of multilayers. Those particles look exactly like the nano-onion fullerenes but with a much larger size and a noteworthy hollow kernel part. The boundary of adjacent COF particles is clear and the hollow centers are not connected. The shape of those COF particles are spheres and ellipses, no rod-like structure is observed in our statistical samples. The author named this new morphology as hollow spherical structure.

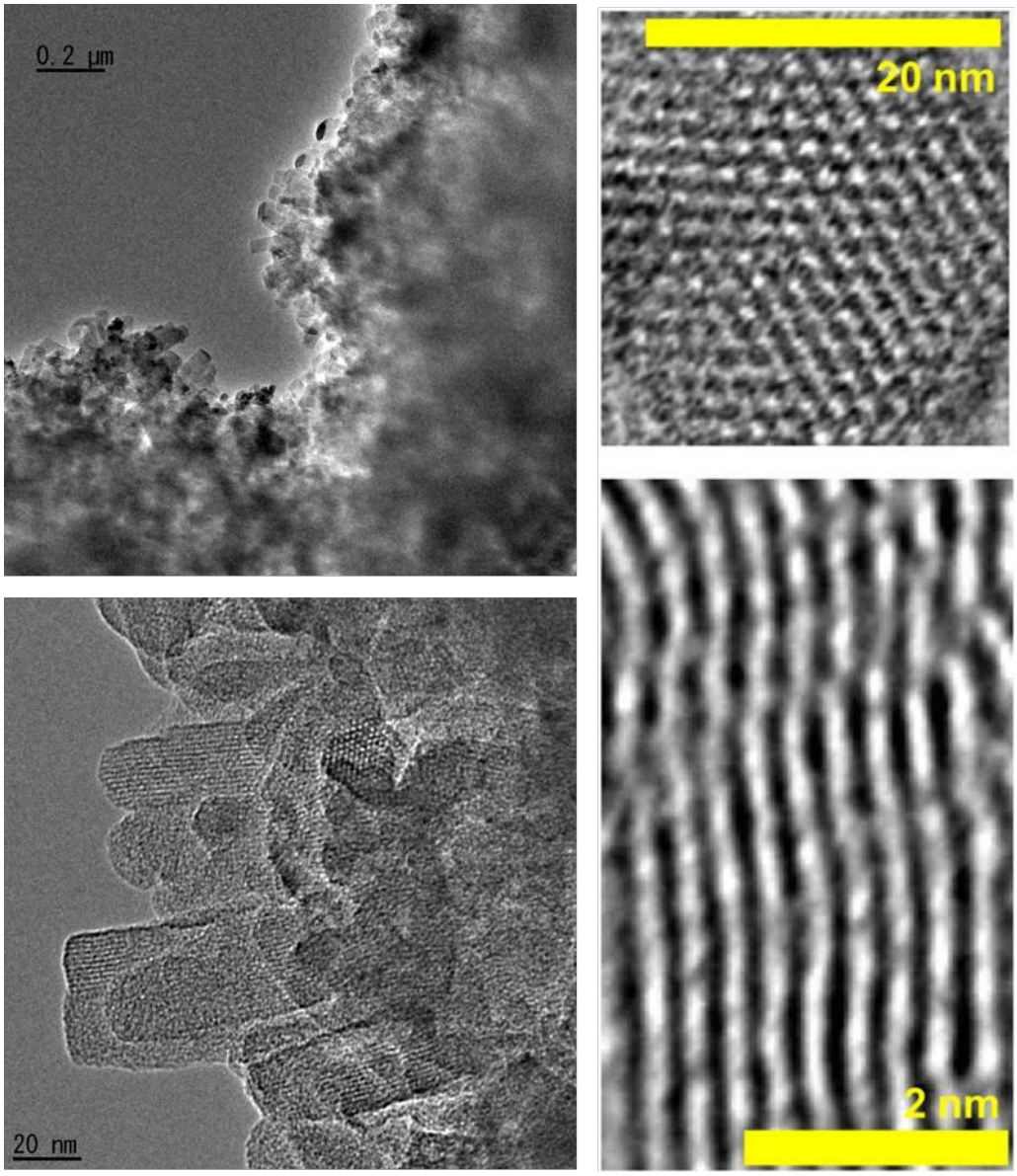

Figure 4. 3. HR TEM images of TPB-DMTP-COF in different magnitudes (upper left: 0.2 *u*m scale; lower left and upper right: 20 nm scale; upper right: 2 nm scale).

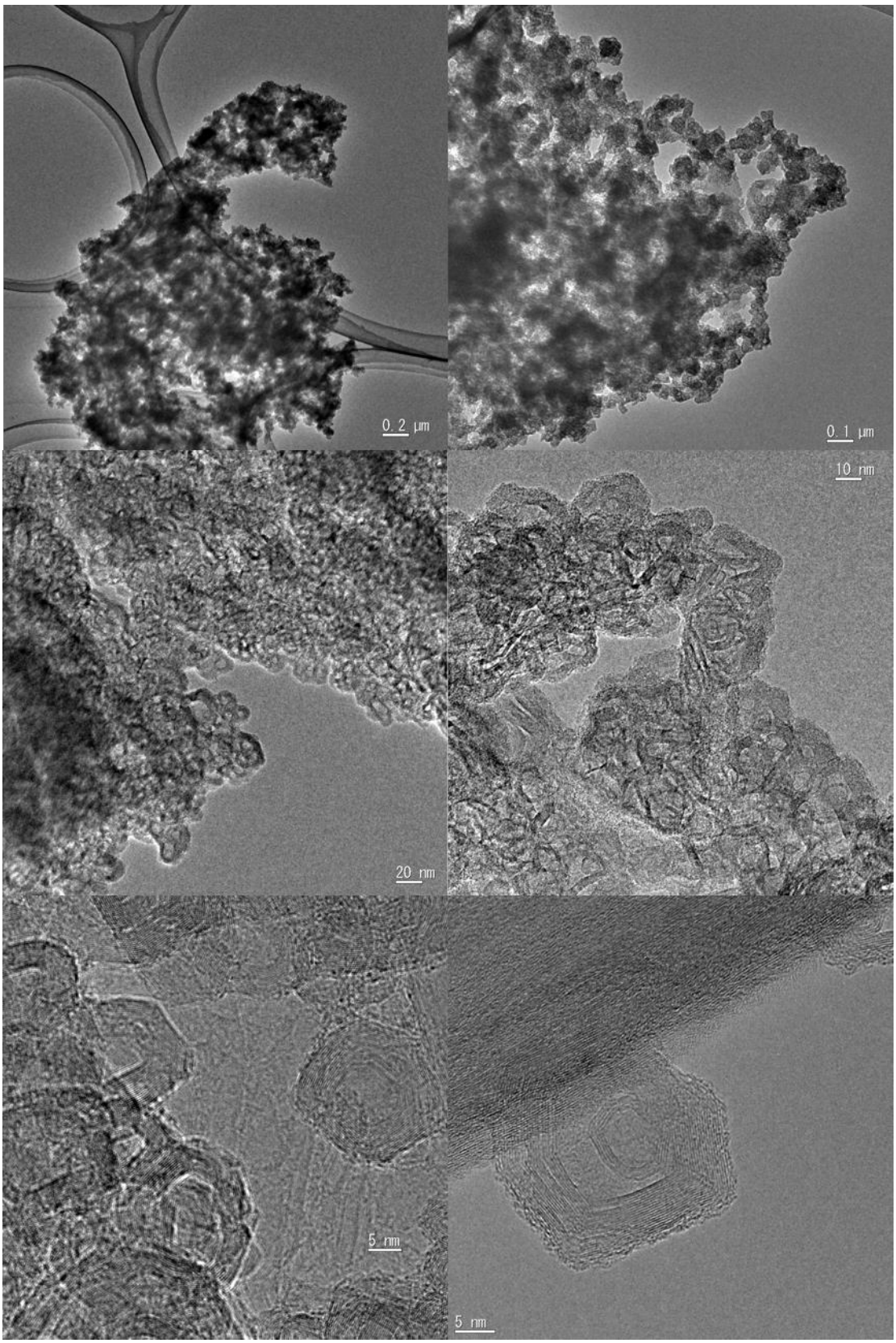

Figure 4. 4. Hollow spherical structure of TPB-DMTP-COF in TEM.

Although most of the hollow spherical structures are small particles with diameters no larger than 0.1 *u*m, some TEM images indeed captured "much larger" sphere particles in rare circumstances **(Figure 4. 5)**. The sphere particles aggregate together as a bunch of grapes with average diameters obviously larger than 0.1 *u*m. Based on the contrast differences of TEM image, we can presume that some particles have solid cores while some of them are hollow structure and the thickness of hollow shells are not homogeneous. The characteristic lattice structure of 2D COF can be observed on the surface of sphere particles under high magnitude. These "larger" sphere particles may share the same origin with the hollow spherical structure with small dimension.

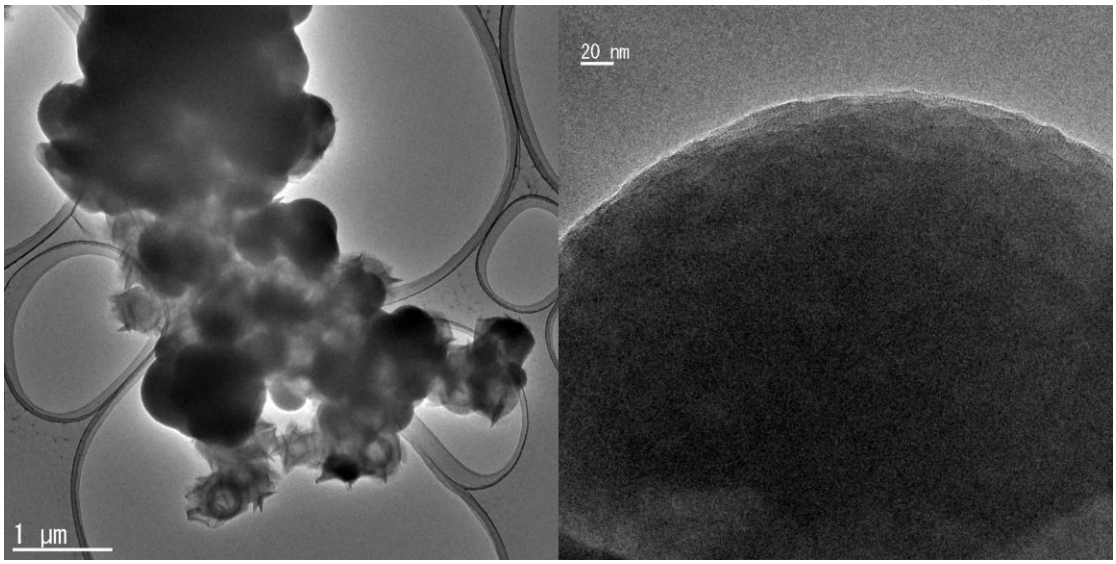

Figure 4. 5. Large sphere particles of TPB-DMTP-COF in TEM.

Scanning electron microscope (SEM) was also adopt to study the structure of TPB-DMTP-COF **(Figure 4. 6)**. In SEM scope, the surface morphology can be observed in three-dimensional perspective. TPB-DMTP-COF sphere particles demonstrated a smooth surface, while the craters on the surface formed by the aggregation of neighboring particles can been clearly seen. Because SEM have a widely variable magnifying range, the observer has a higher possibility to capture the sphere particles with larger size. In **Figure 4. 6**, most of the sphere particles are larger than 1 *u*m, which can be directly observed using polarizing optical microscopy.

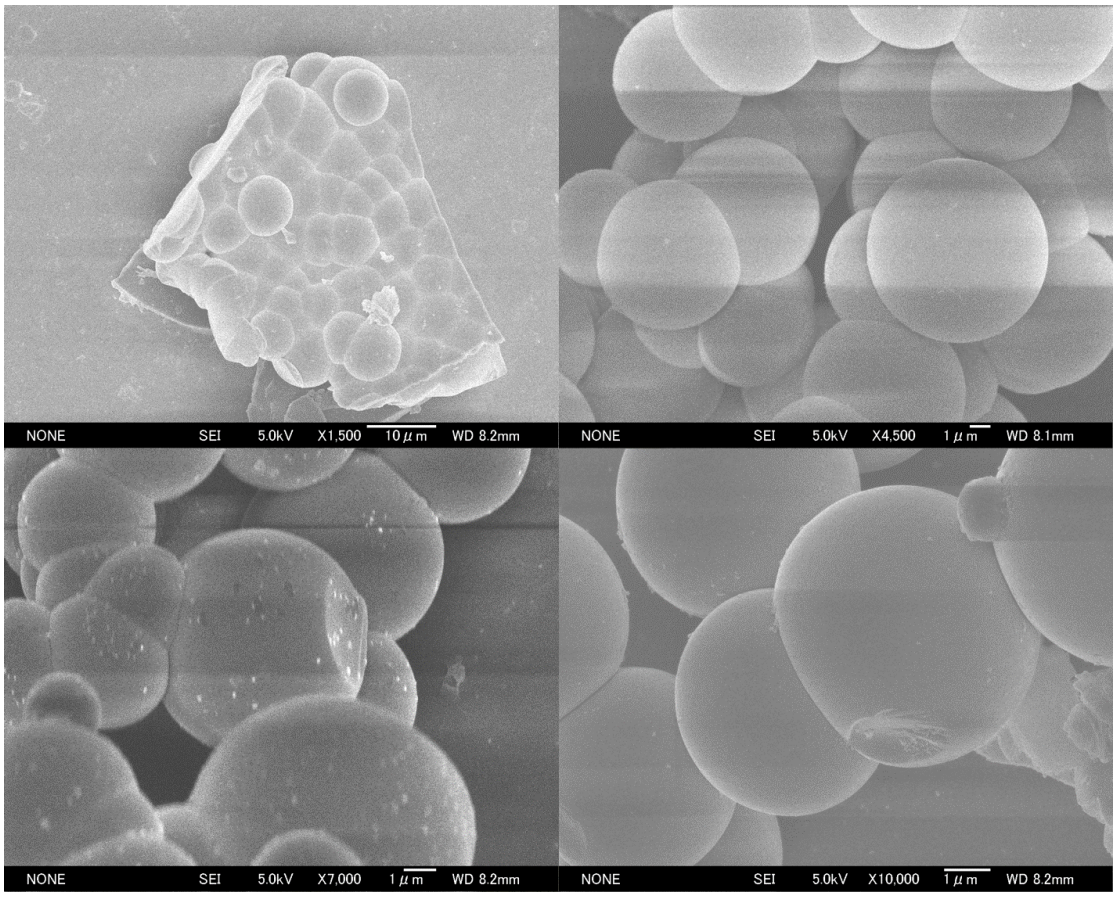

Figure 4. 6. Large sphere particles of TPB-DMTP-COF in SEM.

Anisotropic crystals can be divided into uniaxial crystals and biaxial crystal according to the optical properties. Uniaxial crystals have one optical axis while biaxial crystals have two axes. Based on the material classification in terms of optical properties, hexagonal system crystal belongs to uniaxial crystal. It means that TPB-DMTP-COF has a potential to exhibit characteristic properties as uniaxial anisotropic crystal, which should be observed using PLM technique.

Figure 4. 7. depicts a typical bright field image of TPB-DMTP-COF samples in microscope. Different form the common impression, the powder liked COF samples is not opaque, but partly transparent. COF samples usually emerge two different morphologies in normal light: the lamellar structures with regular sheeted shape and the amorphous phase aggregated as a pile of irregular particles. The presence of the lamellar structure displays the outstanding stability and crystallinity of TPB-DMTP-COF. The amorphous parts imply that 2D COFs can produce unexpected high-order structures under certain conditions.

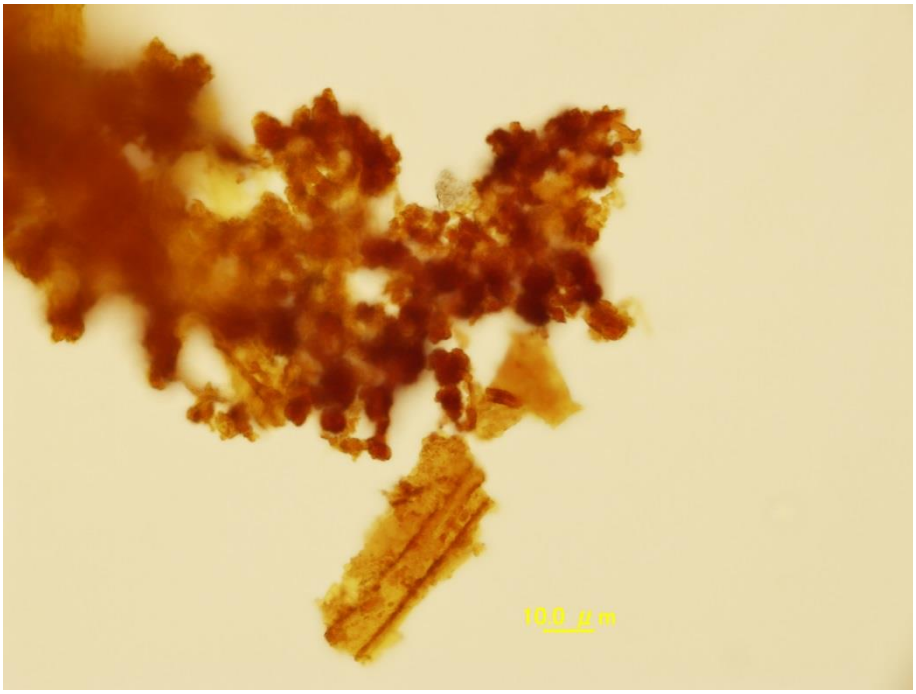

Figure 4. 7. TPB-DMTP-COF samples in bright field scope.

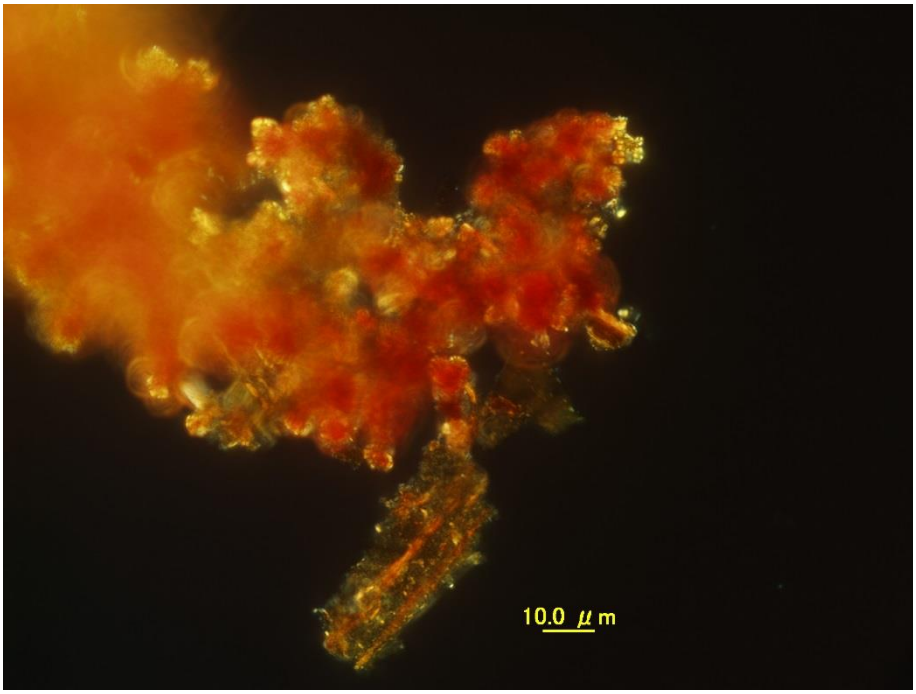

Figure 4. 8. TPB-DMTP-COF samples in polarizing scope.

While switching the optical microscopy to polarizing mode and then a new morphology emerges from the amorphous parts **(Figure 4. 8)**. The new morphology is constituted with small spherical particles of diameters from 1 to 10 um.

These spherical particles give out amber gloss that is much brighter that the amorphous parts in the dark background of polarizing scope. The more important fact is that each spherical particle has a crossed mark formed with dark perpendicular cones and the other parts are colored with brighter regions in between the front. This crossed mark is clearly the Maltese cross and is characteristic of spherulite **(Figure 4. 9)**. This is the first example of spherulite structure of 2D COFs. This also demonstrates the usefulness of polarizing light microscope is successfully applied to studying the optical anisotropy of COF materials.

Based on the difference of birefringence, spherulites can be classify into positive spherulite and negative spherulite. PLM can provide additional structural details for identifying the two types by using test plates. **Figure 4. 10** shows the interference colors image when tint plate (TP530) is inserted into the light path of PLM. The yellow color observed in in quadrant 2 and 4 indicated that TPB-DMTP-COF spherulites are the negative spherulites. These results indicate that the axial refractive index is smaller than tangential refractive index in a spherulite.

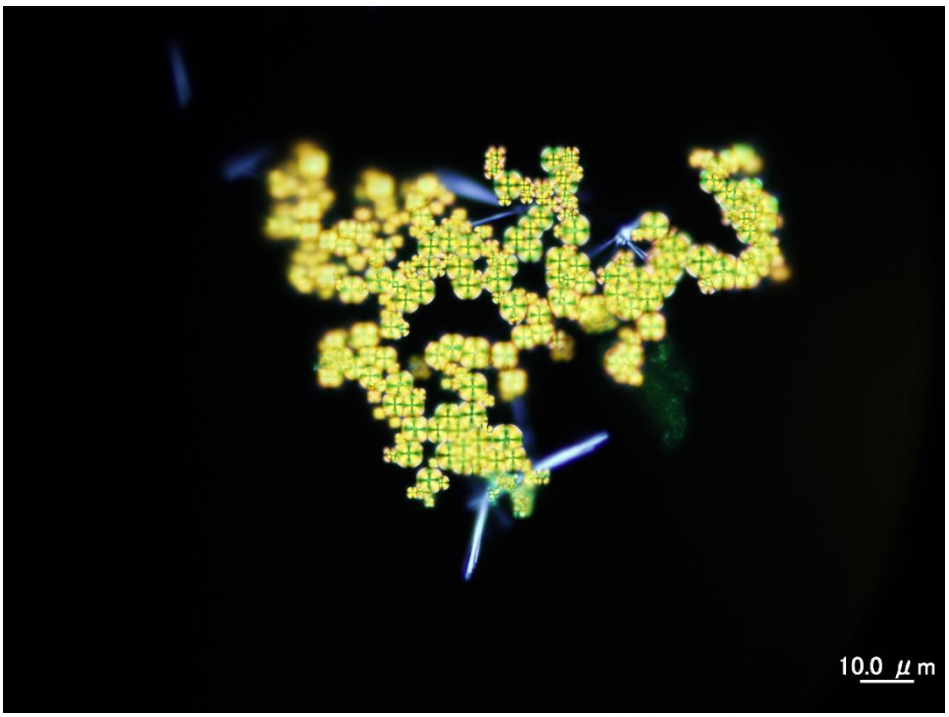

Figure 4. 9. Martese cross in spherulites of TPB-DMTP-COF.

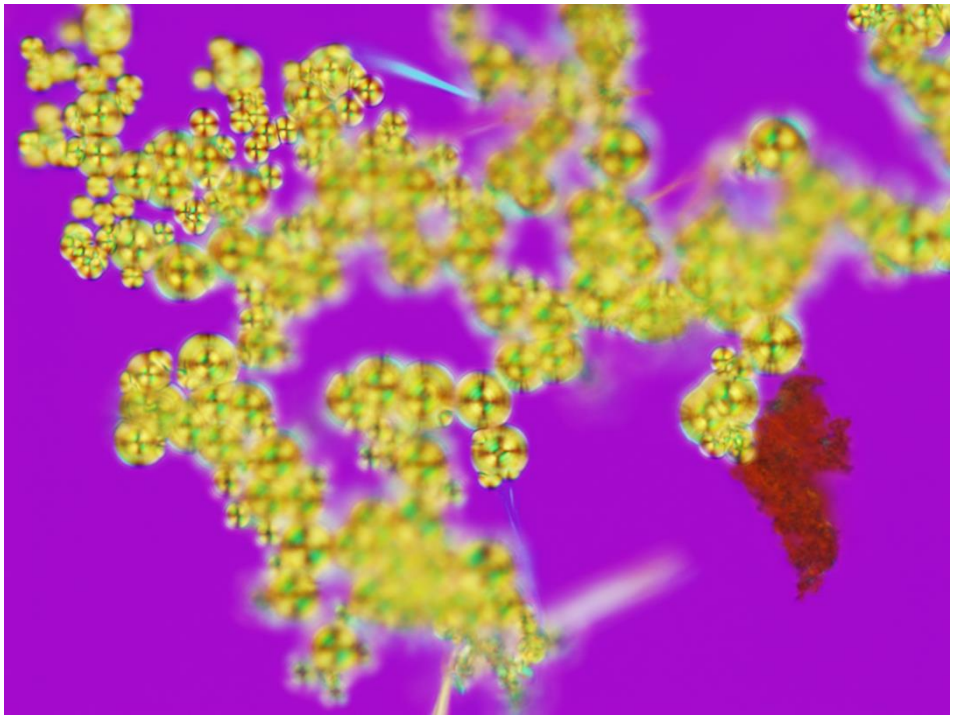

Figure 4. 10. Interference colors in different quadrants of COF spherulites.

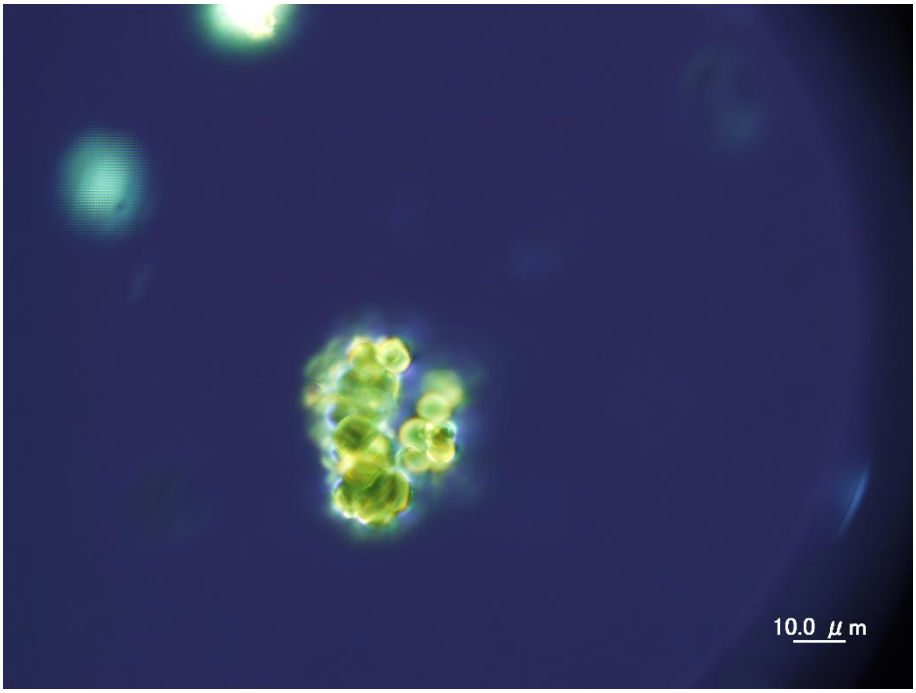

Figure 4. 11. Hollow spherulites in polarizing scope.

Figure 4. 12. Hollow spherulites in interference color with a compensator TP530.

Some of the TPB-DMTP-COF spherulites did not exhibit the Maltese cross emerging in polarizing scope **(Figure 4. 11)**. The author considered that these spherulites may have a relative broader hollow kernel than the spherulites with Maltese cross. Firstly, the brightness of spherulites without Maltese cross is much darker than that with Maltese cross. It is probably because that the thinner shell structure creates relative small optical path difference (OPD), which causes the larger extinction in analyzer. Secondly, when TP530 plate is inserted into the light path, the edge of spherulite still occurs retardation phenomenon and the color change is the same as that of those spherulite with Maltese cross **(Figure 4. 12)**. Therefore, the reason for the disappearance of Maltese cross is that the spherulite is empty that reduces the appearance in optical anisotropy measurements.

The presence of the hollow spherical structure challenges the basic plain structure of 2D COFs. A typical 2D COF such as TPB-DMTP-COF should constitute infinite sheets parallel aligned and each individual layer should consist of only hexagonal rings. However, this 2D structure does not account for the presence of spherical structures in nanometer-sized COF particles.

Based on the concept of reticular chemistry, the hollow spherical structure (nanoparticles and spherulites) formed in TPB-DMTP-COF can be abstracted as assembles of convex polyhedrons with different diameters. For an individual convex polyhedral, a mathematics rule known as Euler's polyhedron formula (**Equation 4. 1**) that describes a topological space's shape or structure regardless of the way it is bent, must be obeyed, where V, E, and F are the numbers of vertices (corners), edges and faces in the given polyhedron, respectively.

$$\boldsymbol{V - E + F = 2} \qquad \textbf{(4. 1)}$$

Based on the Euler's polyhedron formula, one can easily infer that a convex polyhedral cannot be assembled with hexagon alone. A circumstantial evidence is that Euclidean polyhedral only have tetrahedron, hexahedron, octahedron, dodecahedron and icosahedron, which constitute with triangles, quadrangles and pentagons but without hexagon. On the contrary, if a typical 2D COF with hexagonal lattice can form convex polyhedral, such as TPB-DMTP-COF, some polygons other

than hexagon should be formed in the surface that enables the whole closed shell structure and meets the Euler's polyhedron formula. This is the theoretical basis for explaining the existence of 2D COF spherical structure. The only question is whether some other polygons can be proofed to be existed in experiment.

Fortunately, the existence of exotic polygons other than hexagon has been verified using scanning tunneling microscopy (STM) in a series of the experiments about the synthesis of surface covalent organic frameworks[17-19]. For example, Matthew O. Blunt *et al.* demonstrated the formation of polygonal rings with different edges from four to eight in growing 2D covalent networks on a Au (111) substrate[18]. Apparently, hexagonal rings take a predominant amount in bulk polymerization experimental conditions. The existence of other kinds of polygons can not be neglected and those polygonal rings play a key role in forming the hollow spherical structure of 2D COFs. In this sense, the direction observation of such polygon structures of TPB-DMTP-COF samples would provide direct evidence.

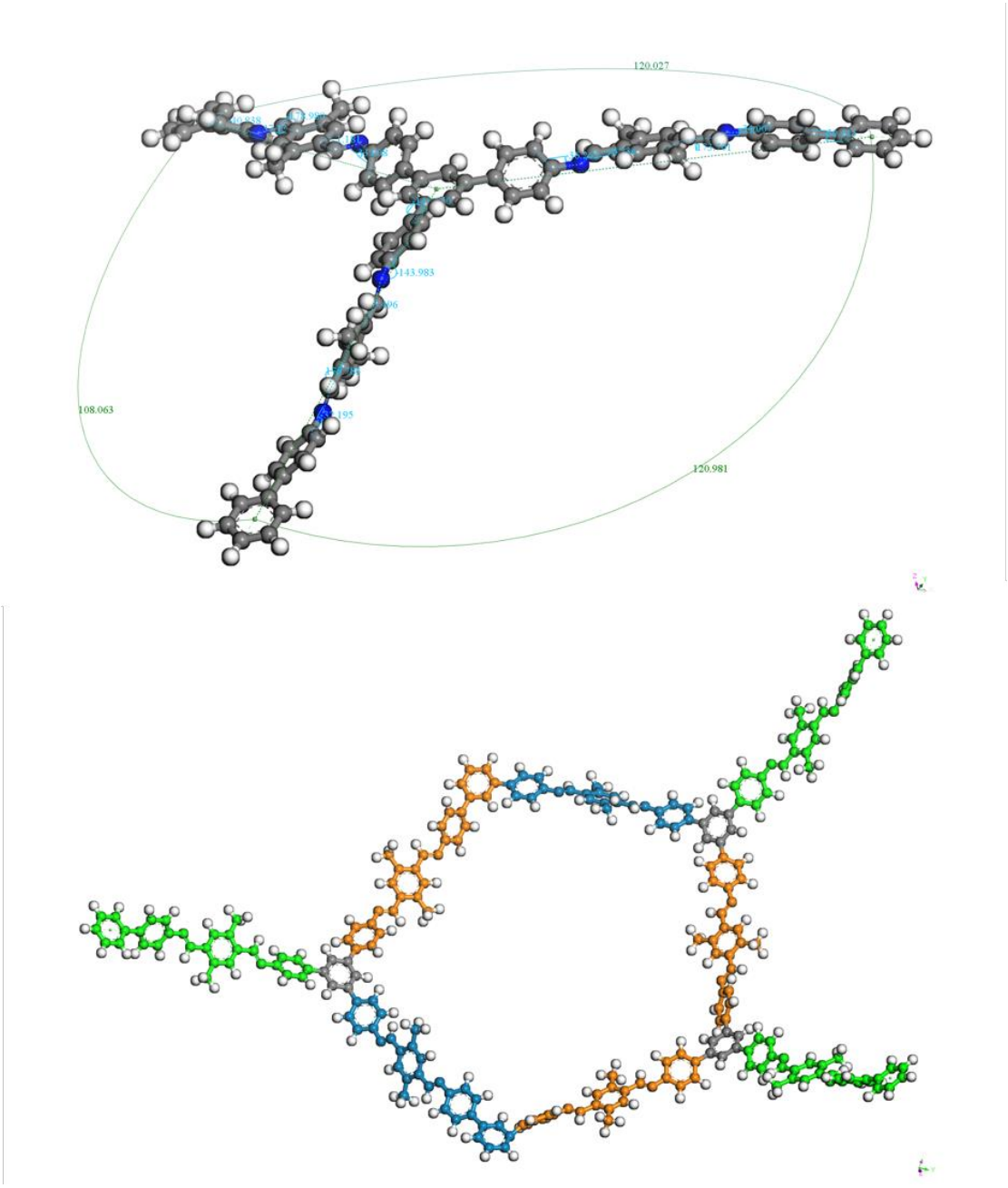

Figure 4. 13. The molecular fragment for constructing the hollow spherical structural models.

Based on the basic concept of geometry, the four and five-membered ring lead to the formation of convex surface and the rings with more than seven members will cause the concave surface such as saddle camber (Discussion about the concave surface is skipped in this thesis because it do not concern with the hollow spherical structure.). Compared to a pentagonal ring, four-membered rings suffer higher structural tension and is to be unfavorable in a thermodynamic view. Hence, the author only adopt pentagonal rings to illustrate the mechanism of hollow spherical structure formation, for simple and clear.

Given the assumption the author proposed above, the convex surface of 2D COF can be transformed to the topology matter with a diagram of trivalent nodes and five and six-membered ring. In this scenario, the analysis methods for fullerene can be referred because 2D COF convex surface and fullerene are equivalent in a topological view. As we know, the structure of a fullerene is a trivalent convex polyhedron with pentagonal and hexagonal faces. In graph theory, the term fullerene refers to any 3-regular, planar graph with all faces of five or six-membered rings. It ought to comply Euler's polyhedron formula **(Equation 4. 1)**, which means that there are exactly 12 pentagons in a fullerene and V/2 − 10 hexagons. Back to the TPB-DMTP-COF's case, the inevitable existence of pentagonal ring formed with the TPB-DMTP-COF edges give rise to the hollow spherical structure in TEM images **(Figure 4. 4)**.

By substituting the C-C bond with TPB-DMTP-COF edges, a series of 2D COF convex surface models can be established. For example, **Figure 4. 14a** presents a schematic diagram of an individual close shell structure of TPB-DMTP-COF with the identical topology of C60. The length of TPB-DMTP-COF edge is about 2.1 nm, so the diameter of the structure model in **Figure 4. 14a** can be roughly estimated at 10 ~11 nm.

Figure 4. 14b demonstrate a multiply layered model for imitating the hollow spherical structure of TPB-DMTP-COF. The influence taken by the pentagon ring is obvious. Based on the discussion in pervious chapter, the pentagon ring as a kind of structural defect for hexagonal lattice, is definitely decrease the quality of PXRD peaks somehow. However, for ideal closed convex surface of 2D COF, there only exist 12 pentagons in one shell, theoretically. The proportion of pentagons of a shell structure declines with the increasing of the curvature radius in inverse square relationship. Therefore, the influence of pentagon ring on PXRD can be neglected in large scale. On the other hand, the adjacent layer/shell is not paralleled in AA, AB or Slipped-AA stacking due to the different curvature radius but in twisted stacking in some way, which cannot decrease the PXRD signals. While in a global view, the formation of hollow spherical structure will show no difference compared with lamellar COF structures in PXRD spectra. This result is also suitable to spherulites of 2D COFs.

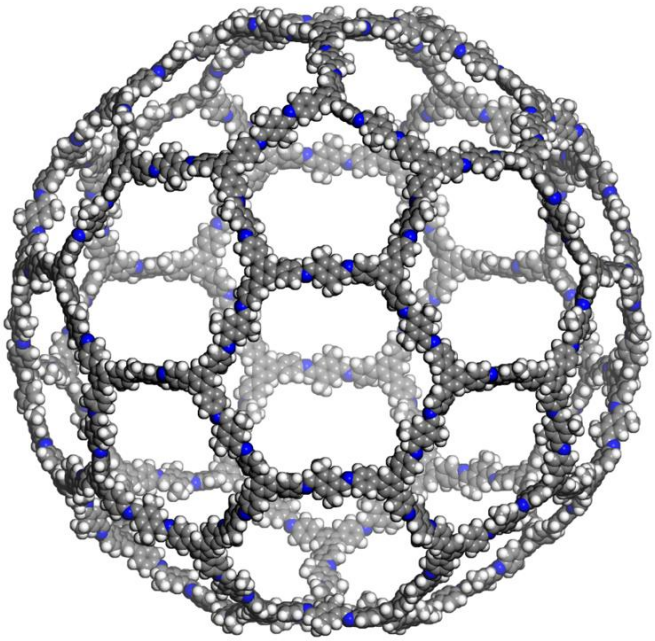

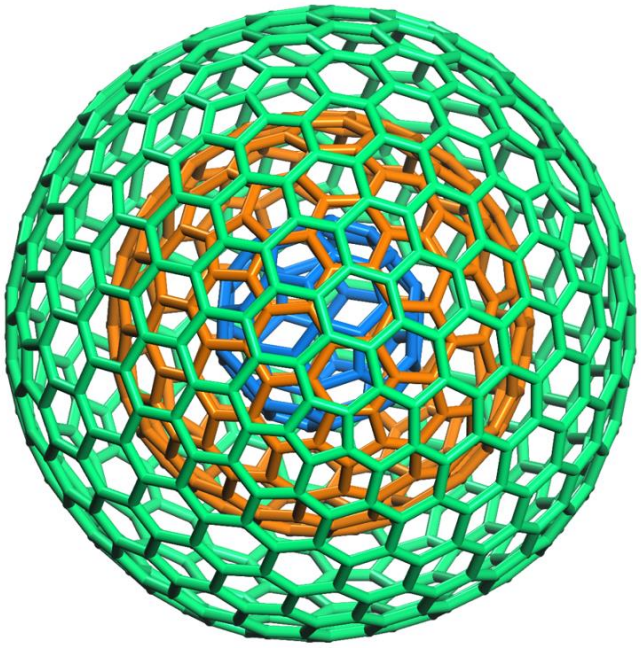

Figure 4. 14. The simulated models of spherical hollow structure of a) analogue structure of C_{60} and b) analogue structure of nano onion $C_{60}@C_{240}@C_{540}$.

4.4 Conclusion

In this chapter, the author confirmed that an imine-linked COF (TPB-DMTP-COF) could form hollow spherical nanoparticles and spherulites. The observation of COF spherulites is a strong proof that COFs have a potential in forming crystalline structures. The author presented a curvature model for elucidating the structure of these hollow spherical structures and matched with the experimental phenomenon very well. The effect of curvature structure on PXRD pattern also discussed.

4.5 References

1) H. Xu, J. Gao and D. Jiang, *Nature Chemistry,* 2015, **7**, 905.

2) A. P. Coˆte´, A. I. Benin, N. W. Ockwig, M. O' Keeffe, A. J. Matzger and O. M. Yaghi, *Science*, 2005, **310**, 1166.

3) A. P. Cote´, H. M. El-Kaderi, H. Furukawa, J. R. Hunt and O. M. Yaghi, *J. Am. Chem. Soc*. 2007, **129**, 12914.

4) S. Wan, F. Gandara, A. Asano, H. Furukawa, A. Saeki, S. K. Dey, L. Liao, M. W. Ambrogio, Y. Y. Botros, X. Duan, S. Seki, J. F. Stoddart and O. M. Yaghi, *Chem. Mater.*, 2011, **23**, 4094.

5) S. Wan, J. Guo, J. Kim, H. Ihee and D. Jiang, *Angew. Chem., Int. Ed.*, 2009, **48**, 5439.

6) R. W. Tilford, W. R. Gemmill, H.-C. zur Loye and J. J. Lavigne, *Chem. Mater.*, 2006, **18**, 5296.

7) E. L. Spitler, B. T. Koo, J. L. Novotney, J. W. Colson, F. J. Uribe-Romo, G. D. Gutierrez, P. Clancy and W. R. Dichtel, *J. Am. Chem. Soc.*, 2011, **133**, 19416.

8) E. L. Spitler, J. W. Colson, F. J. Uribe-Romo, A. R. Woll, M. R. Giovino, A. Saldivar and W. R. Dichtel, *Angew. Chem., Int. Ed.*, 2012, **51**, 2623.

9) S. Kandambeth, A. Mallick, B. Lukose, M. V. Mane, T. Heine and R. Banerjee, *J. Am. Chem. Soc.*, 2012, **134**, 19524.

10) F. J. Uribe-Romo, C. J. Doonan, H. Furukawa, K. Oisaki and O. M.

Yaghi, *J. Am. Chem. Soc.*, 2011, **133**, 11478.

11) X. Feng, L. Liu, Y. Honsho, A. Saeki, S. Seki, S. Irle, Y. Dong, A. Nagai and D. Jiang, *Angew. Chem., Int. Ed.*, 2012, **51**, 2618.

12) S. Jin, X. Ding, X. Feng, M. Supur, K. Furukawa, S. Takahashi, M. Addicoat, M. E. El-Khouly, T. Nakamura, S. Irle, S. Fukuzumi, A. Nagai and D. Jiang, *Angew. Chem., Int. Ed.*, 2013, **52**, 2017.

13) Materials Studio Release Notes v.4.4 (Accelrys Software, 2008).

14) B. Aradi, B. Hourahine and T. Frauenheim, *J. Phys. Chem. A*., 2007, **111**, 5678.

15) B. Lukose, A. Kuc and T. Heine, *J. Mol. Model.,* 2013, **19**, 2143.

16) T. Düren, F. Millange, G. Férey, K. S. Walton and R. Q. Snurr, *J. Phys. Chem. C.*, 2007, **111**, 15350.

17) N. Zwaneveld, R. Pawlak, M. Abe, D. Catalin and L. Porte. L., *J. Am. Chem. Soc.*, 2008, **130**, 6678

18) M. O. Blunt, J. C. Russell, N. R. Champness and P. H. Beton, *Chem. Commun.*, 2010, **46**, 7157.

19) J. F. Dienstmaier, D. Medina, M. Dogru, T. Bein and M. Lackinger, *Acs. Nano.*,2012, **6**, 7234.

Chapter 5

General Conclusion

In this thesis, the author focused on the crystalline structures of two-dimensional covalent organic frameworks, taking on theoretical analysis and experimental studies from three different aspect in spatial scale from nanoscale to macroscale.

In chapter 2, the author studied the host–guest effect between the guest molecules and the channels of 2D COFs in nanoscale. The correlation with the variation of PXRD pattern was discussed and explained the PXRD spectra of as-synthesis COF-1 very well.

In chapter 3, the author proposed a hypothesis for reinterpreting the stacking mode of 2D COFs. The effect of relative rotation of COF layers to PXRD spectra was specified interpreted.

In chapter 4, the author first brought PLM technique to study the crystalline properties of 2D COF in macroscale and discovered the formation of 2D COF spherulites. A coverture model for demonstrating hollow spherical 2D COF structures was built up.

The value of this thesis lies in the insights that it systematic development of a hierarchical multiscale model system for elucidating the crystalline structure of 2D COFs. These results provide powerful tools for the further exploration to the crystalline essence of 2D COFs.

List of Publication

1) Covalent organic frameworks with spatially confined guest molecules in nanochannels and their impacts on crystalline structures

   Jia Gao and Donglin Jiang*

   Chem. Commun., 2016, **52**, 1498.

List of Supplementary Publications

1) Stable, crystalline, porous, covalent organic frameworks as a platform for chiral organocatalysts

   Hong Xu, **Jia Gao** and Donglin Jiang*

   Nature Chemistry, 2015, **7**, 905.

2) Rational design of crystalline supermicroporous covalent organic frameworks with triangular topologies

   Sasanka Dalapati, Matthew Addicoat, Shangbin Jin, Tsuneaki Sakurai, **Jia Gao**, Hong Xu, Stephan Irle, Shu Seki and Donglin Jiang*

   Nature Communications, 2015, **6**, 7786. DOI:10.1038/ncomm8786.

3) A π-electronic covalent organic framework catalyst: π-walls as catalytic beds for Diels–Alder reactions under ambient conditions

   Yang Wu, Hong Xu, Xiong Chen, **Jia Gao** and Donglin Jiang*

   Chem. Commun., 2015, **51**, 10096.

4) Photoelectric covalent organic frameworks: converting open lattices into ordered donor–acceptor heterojunctions

Long Chen, Ko Furukawa, **Jia Gao**, Atsushi Nagai, Toshikazu Nakamura, Yuping Dong and Donglin Jiang*

J. Am. Chem. Soc., 2014, **136**, 9806.

5) Catalytic covalent organic frameworks via pore surface engineering

Hong Xu, Xiong Chen, **Jia Gao**, Jianbin Lin, Matthew Addicoat, Stephan Irle and Donglin Jiang*

Chem. Commun., 2014, **50**, 1292.

6) An azine-linked covalent organic framework

Sasanka Dalapati, Shangbin Jin, **Jia Gao**, Yanhong Xu, Atsushi Nagai and Donglin Jiang*

J. Am. Chem. Soc., 2013, **135**, 17310.

Acknowledgement

I would like to express my deepest appreciation to my supervisor Prof. Dr. Donglin Jiang for offering me the opportunity to do my PhD study in IMS, for the guidance throughout the research process and the review of this work and for giving me the freedom to think independently and pursue my own ideas. It has always been a pleasure to learn from his intuitive scientific understandings.

I would also like to thank all members of the Jiang's laboratory for making this group a vigorous place to work and for fun moments and the fruitful discussions of both scientific and casual topics. It has always been a pleasure to solve the many experimental problems together with them when I cannot deal with alone. Among all of them, I want to express my especially thanks to Mr. Enquan Jin, Dr. Hong Xu and Dr. Sasanka Dalapati, my main collaborators and coauthors as shown in the publication list. Many thanks for your advice and most importantly your friendship.

I gratefully appreciate the scholarship of Chinese Scholarship Council (CSC) for supporting my study in Institute for Molecular Science, Okazaki, Japan during the past three years.